



Bactericidal coating to prevent early and delayed implant-related infections

F. Jahanmard^{a,1}, M. Croes^{a,1}, M. Castilho^{a,b}, A. Majed^a, M.J. Steenbergen^c, K. Lietaert^{d,e},
H.C. Vogely^a, B.C.H. van der Wal^a, D.A.C. Stapels^f, J. Malda^{a,g}, T. Vermonden^c, S. Amin Yavari^{a,*}

^a Department of Orthopedics, University Medical Center Utrecht, Utrecht, the Netherlands

^b Department of Biomedical Engineering, Eindhoven University of Technology, Eindhoven, the Netherlands

^c Department of Pharmaceutics, Utrecht Institute for Pharmaceutical Sciences (UIPS), Utrecht University, Utrecht, the Netherlands

^d 3D Systems - LayerWise NV, Leuven, Belgium

^e Department of Metallurgy and Materials Engineering, KU Leuven, Leuven, Belgium

^f Department of Medical Microbiology, University Medical Center Utrecht, Utrecht, the Netherlands

^g Department of Clinical Sciences, Faculty of Veterinary Medicine, Utrecht University, Utrecht, the Netherlands

ARTICLE INFO

Keywords:

Orthopedic implant
Infection
Drug delivery
Electrospinning
Additive manufacturing

ABSTRACT

The occurrence of an implant-associated infection (IAI) with the formation of a persisting bacterial biofilm remains a major risk following orthopedic biomaterial implantation. Yet, progress in the fabrication of tunable and durable implant coatings with sufficient bactericidal activity to prevent IAI has been limited. Here, an electrospun composite coating was optimized for the combinatorial and sustained delivery of antibiotics. Antibiotics-laden poly(ϵ -caprolactone) (PCL) and poly(L-lactic-co-glycolic acid) (PLGA) nanofibers were electrospun onto lattice structured titanium (Ti) implants. In order to achieve tunable and independent delivery of vancomycin (Van) and rifampicin (Rif), we investigated the influence of the specific drug-polymer interaction and the nanofiber coating composition on the drug release profile and durability of the polymer-Ti interface. We found that a bi-layered nanofiber structure, produced by electrospinning of an inner layer of [PCL/Van] and an outer layer of [PLGA/Rif], yielded the optimal combinatorial drug release profile. This resulted in markedly enhanced bactericidal activity against planktonic and adherent *Staphylococcus aureus* for 6 weeks as compared to single drug delivery. Moreover, after 6 weeks, synergistic bacterial killing was observed as a result of sustained Van and Rif release. The application of a nanofiber-filled lattice structure successfully prevented the delamination of the multi-layer coating after press-fit cadaveric bone implantation. This new lattice design, in conjunction with the multi-layer nanofiber structure, can be applied to develop tunable and durable coatings for various metallic implantable devices. This is particularly appealing to tune the release of multiple antimicrobial agents over a period of weeks to prevent early and delayed onset IAI.

1. Introduction

The significant increase in life expectancy has resulted in a steep rise in orthopedic and dental implant applications during the past decades [1–4]. Implant-associated infections (IAI) are a major complication of such implant usage [5,6], and can either arise from perioperative wound contamination, infections in nearby body sites that reach the implant, or via hematogenous spreading of bacteria from a more distant infection site to the implant [7]. The eradication of the dense and matrix-rich bacterial biofilm that forms on the implant surface is one of the biggest challenges for orthopedic patients and surgeons [8]. The only treatment modality that remains is an aggressive one, composed of multiple surgeries to remove the infected implant and sterilize the

wound bed, in combination with prolonged systemic antibiotics treatment. The associated patient morbidity and costs are extremely high, typically reaching \$50,000 per case in a complicated scenario [9].

Local delivery of antibiotics in the direct vicinity of the implant allows for the highest achievable antibacterial activity at the required site, while reducing the chance of systemic toxicity [10]. Current approved local delivery systems have suboptimal efficacy and a poor tunability in terms of combinatorial drug selection and their delivery [11,12]. For improved controllability of the drug release [13], various antibacterial coating strategies have been explored [6,14], whereby the antimicrobial molecules are locally-delivered through physical adsorption [15], encapsulation in a polymer matrix [16] or chemical conjugation [17]. Despite these technological advances, the current

* Corresponding author at: Department of Orthopedics, University Medical Center Utrecht, Utrecht 3508GA, the Netherlands.

E-mail address: S.AminYavari@umcutrecht.nl (S. Amin Yavari).

¹ Authors contributed equally

<https://doi.org/10.1016/j.jconrel.2020.06.014>

Received 19 March 2020; Received in revised form 22 May 2020; Accepted 14 June 2020

Available online 21 June 2020

0168-3659/ © 2020 The Authors. Published by Elsevier B.V. This is an open access article under the CC BY license (<http://creativecommons.org/licenses/by/4.0/>).

efforts overly focus on biofilm prevention in the immediate post-operative window, and neglect the possibility of delayed infections originating from a remote infection source [18,19]. As such, IAI can originate after direct contamination of the implant during surgery or via the spread from nearby infected tissue. These types of infections are respectively denoted as early and delayed infections, whereby delayed infections have been defined as having an onset 2–12 weeks after the surgery, depending on the orthopedic application [19,59]. Based on this, one could argue that preventive strategies should ideally aim at the release of antibiotics for even several months [11]. On the other side of the coin, however, one should consider the inevitable risk of antimicrobial resistance development when administering antibiotics over an excessive period of time. As 6 weeks of antibiotic treatment is a well-accepted standard treatment modality to treat IAI [60], a local drug release of approximately 6 weeks can be considered ideal for newly developed prophylactic antibacterial implant coatings.

The occurrence of antibiotic-resistant bacteria is another concern. They are more likely to surface when local antibiotic concentrations are not sufficiently high [20]. Intuitively, the chance of developing antibiotic resistant strains is decreased if complete bacterial eradication would be achieved. For that, combinatorial antibiotics treatment has proven to be superior to single drug treatment [21]. Patients with IAI frequently present with methicillin-resistant *Staphylococcus aureus* (MRSA) [22], supporting the use of vancomycin (Van) with efficacy against planktonic MRSA [23] as a first arm in combinatorial drug delivery systems. At the same time, clinical evidence suggests an excellent antibacterial efficacy of rifampicin (Rif) towards *staphylococci* and their biofilms [21,24]. However, its widespread clinical use is being endangered by the emergence of Rif resistant mutants, particularly when Rif is used as a monotherapy [25]. Local drug delivery systems should therefore ensure efficient co-delivery of Rif with other broad-range antibacterial drugs for maximal antibacterial efficacy. In this respect, an antibacterial coating that comprises a combinatorial Van/Rif delivery opens promising avenues.

Current implant coatings to prevent IAI fall short because of limited bio-stability or durability, single functionality and/or lack of tunable delivery of active agents [26,27]. Electrospinning technology offers potential to tackle these issues, as it allows for high encapsulation and drug loading efficiencies [28,29], and the ability to create coatings with adjustable physical (e.g. microstructure and porosity) [30,31] and chemical (e.g. type of polymers, solvent and biomolecules) [32] nanofiber properties. With this respect, several electrospun mats are already reaching clinical practice, as they allow for sustained drug release, are malleable, and can be incorporated into existing wound dressings or vascular devices [33,34]. Due to high antibiotic loading efficiency and long-term release, antibiotic-laden electrospun implant coatings have also shown feasibility to mitigate IAI [35–37]. As a limitation, these strategies have generally only applied a single type of antibiotic, whereas current clinical guidelines recommend combinatorial antibiotic therapy due to higher effectiveness and reduced chance of antibiotic resistance development [21]. At the same time, combinatorial antibiotic approaches have not sufficiently addressed the clinical need for long-term bactericidal properties [18,34,38]. As a relatively unexplored field, electrospinning of certain polymer blends can lead to tailored and prolonged drug release rates [39]. In addition, different fabrication methods (e.g. simple electrospinning or co-spinning) [40–42] can lead to desired structures and properties for different applications. In addition to a necessity of control over (multiple) drug release for a prolonged period (*i.e.* the tunability), the antimicrobial coating methods for metallic implants to date [37,43,44] have exposed an unmet need in sufficient bonding between the implant and the coating to withstand surgical delamination (*i.e.* the durability).

Here, we developed an electrospun nanofiber coating that is compatible with titanium implants, and that provides a combinatorial release of Rif and Van antibiotics. To maximize the durability of the coating, multi-layer nanofibers were electrospun onto microporous

(lattice) structure titanium implants to create nanofiber-filled lattices (NFL). This NFL design eliminates the need of an additional heat or chemical treatment step to produce a durable coating. The feasibility of a bi-layered PCL/PLGA composite was investigated, as they are compatible with many drugs, with the possibility of long-lasting drug release thanks to their slow degradation rates. More importantly, they have a proven biocompatibility and flexible mechanical properties for orthopedic applications [45,46]. To realize a tunable coating, we investigated the influence of nanofiber coating composition, namely either a bi-layered or a core-shell structure, on the kinetics of antibiotic release. These electrospinning methods were compared side-by-side, as both methods can be used to achieve independent release of multiple drugs [47]. Using these methods, it was investigated whether the application of PLGA/Rif as a protective outer layer or shell could control the burst release of Van from the inner PCL/Vanlayer or core.

2. Materials and methods

2.1. Production of lattice structured implants by 3D-printing and morphological characterization

Rod-shape titanium implants (length = 10 mm, diameter = 1.2 mm) with a lattice structure were designed with Magics (Materialise, Leuven, Belgium). The unit cell had a rhombic dodecahedron geometry and a size of 0.8 mm (Fig. 1a). For 3D-printing, Direct Metal Printing (DMP) was used to fabricate the lattice structure implants (Fig. 1b) with a ProX DMP 320 machine (3D Systems, Leuven, Belgium). The titanium powder used for implant manufacturing had a spherical shape and meets ASTM F67 chemical composition Grade 1. An inert gas atmosphere (Argon 5.0) with oxygen concentrations below 50 ppm was applied. After DMP, the implants were manually removed from the support structures (Fig. 1c) followed by a cleaning procedure in demineralized water in an ultrasound bath for 15 min. For morphological characterization, MicroCT (Quantum FX; PerkinElmer, USA) images were acquired with a tube voltage of 90 kV, a tube current of 180 mA, and a field of view of 10 mm. The images were represented as a stack of 2D TIFF images with a resolution of 20 μm . Morphological analyses were performed with the BoneJ plugin (version 1.3.12) in ImageJ freeware version 1.48 (U.S. National Institutes of Health) and yielded a lattice structured implant with a porosity of 50% and an average pore size of $216 \pm 73 \mu\text{m}$ [48].

2.2. Solution electrospinning

To prepare poly (lactic-co-glycolic acid) (PLGA) and polycaprolactone (PCL) solutions, PLGA (50:50 monomer ratio, Corbion, The Netherlands) and PCL (PURASORB PC 12, Corbion, The Netherlands) were dissolved in tetrafluoroethylene (TFE, Sigma, Germany) to 20 w/v%. Rifampicin (Rif, Sigma, Germany) and vancomycin hydrochloride (Van, Sigma, Germany) were dissolved in chloroform (VWR, France) and dimethyl sulfoxide (DMSO, Merck, Japan) to stock concentrations of 150 and 250 mg/ml, respectively. The dissolved Rif and Van were added to the polymer solutions to reach final concentrations of 10 and 30 mg Rif/ml PLGA solution, and 1, 10, 30, 50, and 100 mg Van/ml PCL solution. These concentration ranges were based on initial pilot experiments, which showed that higher concentrations of Rif induced unwanted changes in nanofiber morphology to micro-particles during the electrospinning process. Moreover, a Rif concentration below 10 mg/ml was excluded from experiments, as it resulted in its rapid burst release, making it inappropriate for the purpose of preventing delayed onset infection.

An in-house built uniaxial and coaxial solution electrospinning (SES) system, (Fig. 1e), was employed to coat the drug-laden nanofibers onto lattice structured Ti implants. The polymer/drug solutions were loaded into 1 ml syringes fitted with a 27-gauge (G) needle for uniaxial electrospinning. A voltage of 16 kV (Heinzinger, Germany) was applied

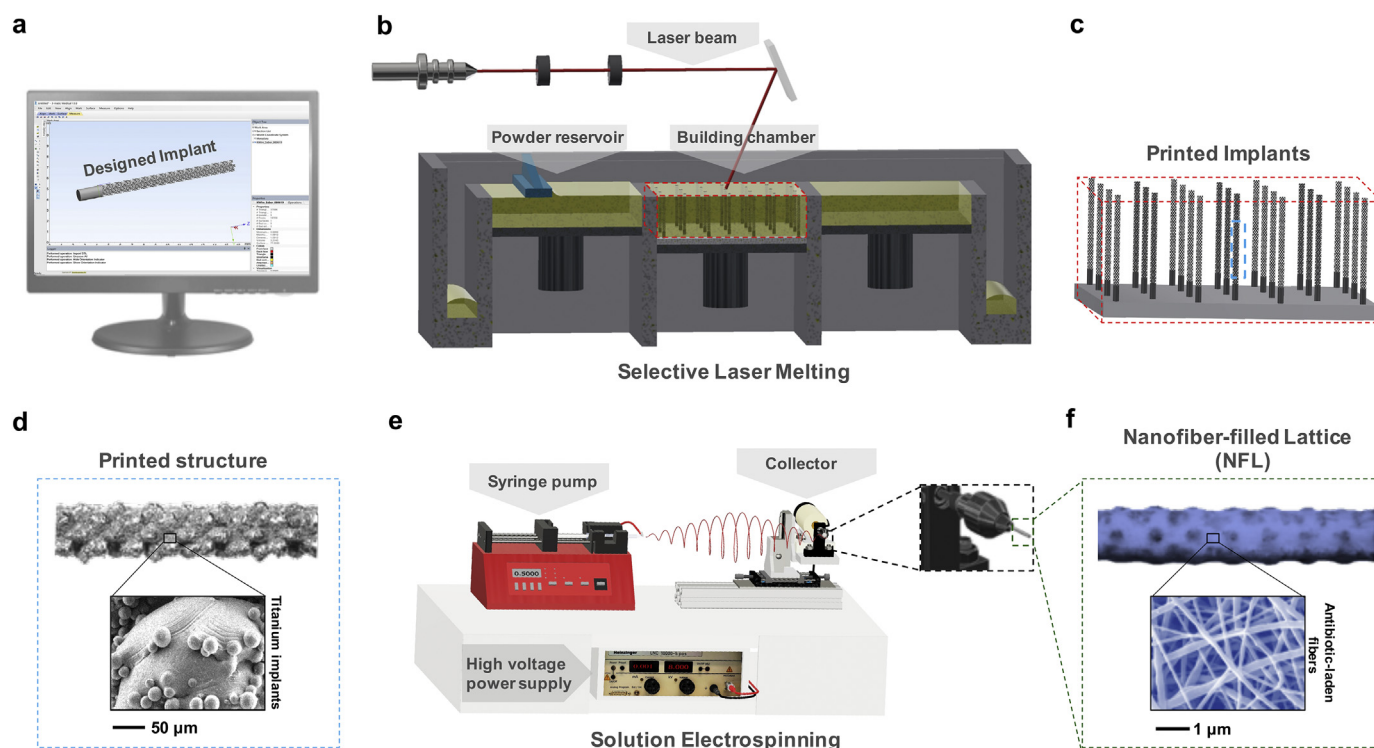


Fig. 1. Process of nanofiber-filled lattice (NFL) implant manufacturing. To produce an implant structure with improved compatibility with electrospun nanofiber coatings, Ti implants with a diamond lattice structure were designed (a) and fabricated (b) by direct metal printing (DMP). (c) The final rod-shape implants had a length of 10 mm and a diameter of 1.2 mm. (d) The unit cell consisted of a rhombic dodecahedron geometry with a size of 0.8 mm. (e) A uniaxial and coaxial solution electrospinning system was made in-house to coat the antibiotics- PCL/PLGA nanofibers onto the lattice structured implants, denoted as NFL implants. (f) Different NFL implant structures were produced with various types of drug-laden nanofibers and fiber assemblies.

between the needle and the implant and a syringe pump (World precision instruments, US) was used to feed the polymer/drug solutions through the needle at a flow rate of 0.5 ml/h. The nanofibers were collected directly onto the implants at a distance of 8 cm from the needle. The resulting coated implants were denoted as nanofiber-filled lattice (NFL) implants.

Different NFL implants were fabricated, for which the applied total thickness of the coatings was chosen to support comfortable press-fit implantation in cadaveric bones, i.e. corresponding to 10 mg total weight of the coating. Single-layer structures were produced by uniaxial SES, denoted as the PCL/Van and PLGA/Rif groups. Bi-layered structures were produced by uniaxial SES of an inner layer of PCL/Van and an outer layer of PLGA/Rif, denoted as the bi-layered group. Core-shell structures were produced by coaxial electrospinning, where the two solutions were independently injected through a coaxial nozzle with inner/outer diameters determined by 20G/14G needles, using a maximum flow rate of 0.5 ml/h and a voltage of 16 kV. Based on TEM characterization, the flow rate ratio was optimized to 2:1 (shell:core) to produce the most uniform core-shell structures. The electrospun samples were dried in a vacuum desiccator for 1 week prior to any experiments to remove possible residual solvents [49].

2.3. Material characterization

The surfaces of the NFL implants were visualized using a scanning electron microscope (SEM, FEI NovaNano, US) after gold sputtering for 30 s. Images were taken at 5.0 kV using a 5-mm working distance. The fiber size and its distribution were measured for three independent samples per group ($n = 100$ fibers/sample) using ImageJ (National Institutes of Health, US). Attenuated total reflection-Fourier transform infrared spectroscopy (ATR-FTIR, Nicolet™ iS™ 10, Thermo Fisher, US) was used to obtain absorbance spectra of drug-laden fibers over 600–4000 cm^{-1} . The nanofibers were mounted on a sample stage and

contacted with an ATR-crystal for FTIR measurement. To visualize the core-shell nanofiber structure, transmission electron microscopy (TEM, FEI Tecnai 12, ThermoSystems-FEI, The Netherlands) was used. For this purpose, a thin layer of nanofibers was electrospun on Formvar-coated grids with a carbon layer. A drop shape analysis system (OCA 15EC, Dataphysics, Germany) was used to calculate the water contact angle of a 10 μL water volume dropped onto the nanofiber surface. The water contact angle was calculated by SCA software (SCA20 module, Dataphysics, Germany). The average water contact angle was reported for five measurements performed on each sample. The mechanical properties of the nanofibers were measured by a universal testing machine (5566, Instron, US) with a 100 N load cell, at a crosshead rate of 10 mm/min and continued until the samples totally failed. For each nanofiber, five rectangular strips (5×20 mm nanofiber matrix) were used for mechanical testing and the average young modulus was exported from the slope of the first linear part of the strain-stress curve. This protocol followed the ASTM D882 standard, suitable for tensile testing of films with a thickness below 1 mm [50–52].

2.4. In vitro release profiles of the antibiotics

The antibiotics release kinetics were characterized by placing the NFL implants in 500 μL of PBS (pH 7.4) at 37 °C. The supernatant was refreshed after 1, 3, 5, 7, 10, 14, 21, 28, 35, and 42 days and stored at -20 °C until analysis. Drug concentrations in the release media were measured using an ACQUITY UPLC H-Class PLUS Bio system (Waters Corporation, US) equipped with a BEH C18 Column (1.7 μm , 2.1 mm \times 50 mm) and a Waters 2996 PDA detector. The elution was carried out with a mobile phase of MilliQ water (MQ, Millipack 40 filter, Merck, Germany) and acetonitrile (ACN, Acetonitrile HPLC gradient, Sigma, Germany) at a MQ/ACN ratio of 95/5, both mixed with 0.1% Trifluoroacetic acid (TFA, Sigma, Germany). A flow rate of 1 ml/min at room temperature and a linear gradient elution program were

used for 4 min. Concentrations of the drugs were quantified using wavelengths for Van (233 nm) and Rif (264 nm) and normalized against a calibration curve obtained by diluting stock solutions of Rif (1 mg/ml in ACN) and Van (1 mg/ml in MQ) in PBS to cover a range of 0.5 to 250 µg/ml. To determine the total drug loads, the nanofiber coatings were dissolved in 250 µL tetrahydrofuran (THF, Sigma, Germany) and 250 µL PBS was added and vortexed for 60 s to precipitate the polymer. The solution was centrifuged at 20,000 ×g for 5 min to pellet any precipitate, and the supernatant was used for determination of the Rif and Van concentrations by HPLC as aforementioned. The amounts of loaded Van were 573.38 ± 21.28 mg (core-shell [PCL/Van]/[PLGA/Rif]), 564.69 ± 17.87 mg (bi-layered [PCL/Van]/[PLGA/Rif]), and 972.12 ± 45.33 mg (PCL/Van). The amounts of loaded Rif were 570.3 ± 44.3 mg (core-shell [PCL/Van]/[PLGA/Rif]), 619.57 ± 25.41 mg (bi-layered [PCL/Van]/[PLGA/Rif]), and 951.5 ± 58.99 mg (PLGA/Rif). The drug in the release media was normalized to the total drug content to determine the cumulative release curves.

2.5. Ex vivo coating durability

The ability of the bi-layered coatings to withstand surgical implantation was evaluated following their implantation into cadaveric rat tibiae, using a surgical procedure that has been reported before [53]. Solid and lattice implants were coated with a bi-layered structure composed of PCL/Van labeled with FITC (Sigma, Germany) and PLGA/Rif labeled with Rhodamine B (Sigma, Germany). The coating morphology was detected by confocal (Leica SP8X, Germany) and stereo microscopy (Olympus SZX16, Germany). In addition, samples were processed for bone staining by basic fuchsin and methylene blue, as previously described [54].

2.6. In vitro antibacterial assay

To assess the antibacterial activity of the NFL implants, *Staphylococcus aureus* strain ATCC 49230 was used. This strain was originally isolated from an osteomyelitis patient, and is also commonly used in animal osteomyelitis models [55]. The bacteria were cultured in fresh tryptic soy broth (TSB) supplemented with 1% glucose at 37 °C and 200 rpm for 24 h and then re-suspended and diluted in TSB to $OD_{600} = 0.01$ (about 10^7 CFU/ml). One ml of this bacterial suspension was added to each sample and kept at 37 °C for 24 h while being continuously stirred at 200 rpm. For later time point assessments (i.e., day 7, 14, 28 and 42), the samples were first kept in PBS at 37 °C to allow drug elution until the preceding day of bacterial quantification (i.e., 6, 13, 27 and 41 days), and were subsequently exposed to the bacterial suspension for 24 h as aforementioned. After 24 h of incubation at 37 °C in a humidified atmosphere, the number of liquid-growing (i.e. planktonic) and implant-adherent bacteria were quantified by plating serial dilutions of the bacterial suspension and counting the colony forming units (CFUs). To remove and quantify implant-adherent bacteria, implants were washed three times in PBS, transferred to a new tube with 2 ml PBS, and sonicated for 1 min. CFU present in the resulting suspension were enumerated as mentioned above. All experiments were performed in triplicate.

To evaluate the zone of inhibition, trypticase soy agar plates were inoculated with 0.5 ml bacterial suspension prepared at $OD_{600} = 0.01$ (about 10^7 CFU/ml) to yield a bacterial lawn. The implants were placed on the plates, which were then incubated for 24 h at 37 °C to visualize the zone of inhibition of bacterial growth. For the later time points (i.e., day 7, 14, 28 and 42), the implants were first kept in PBS at 37 °C to allow drug elution as mentioned above. For imaging of live and dead bacteria, samples were stained with 6 µM SYTO 9 (Thermo Fisher, US) and 20 µg/ml propidium iodide (PI, Thermo Fisher, US) in Hank's Buffered Saline Solution (HBSS, Lonza, Belgium) for 30 min at room temperature. The samples were incubated for 24 h at 37 °C and rinsed

with HBSS before confocal microscopy imaging of live (green) and dead (red) cells. A confocal microscope (Leica TCS SP5 II, Germany) with hybrid detectors that collect fluorescence signal from SYTO 9 (500–550 nm) and PI (600–700 nm), which were given pseudo colors in the images, was used for this study.

2.7. In vitro cell biocompatibility

Following other reports [56,57], NFL implants were sterilized by UV radiation for 1 h and washed three times with PBS for 5 min prior to any cell culture experiments. UV-treated samples were occasionally incubated in cell culture medium without antibiotics, which confirmed their sterility. MC3T3-E1 pre-osteoblast cells (ATCC, Germany) were cultured in growth medium consisting of α-MEM (Invitrogen, US) supplemented with 10% fetal bovine serum (FBS, Biowest, France) and 100 units/ml penicillin/streptomycin (Invitrogen). The cells were seeded onto the implants in a 12-well plate at a density of 2×10^5 cells/well in growth medium at 37 °C, 5% CO₂ and 95% humidity. The biocompatibility of the different NFL implants was evaluated with the Alamar blue metabolic activity assay over a period of 14 days, by transferring the implants to a new well and incubating them with 10% of AlamarBlue Cell Viability Reagent (Thermo Scientific, US) in growth medium. The fluorescence at 544/590 nm was detected using a Fluoroskan Ascent FL multiplate reader (Thermo Labsystems, Finland) after 4 h. The cytocompatibility of the coated implants was evaluated with a Live-Dead cell staining kit (Molecular Probes, Thermo Scientific, US) after 7 and 14 days following the manufacturer procedure. Using a confocal microscope (Leica SP8X, Germany), hybrid detectors collected the fluorescence signal from live (green) (500–525 nm) and dead (red) (528–640 nm) cells, which were given pseudocolours in the images. Z-stack images were processed using Leica LASX acquisition software to create single maximum projections. The number of live and dead cells were counted for three images/group using ImageJ software, and their relative percentages were reported.

To assess changes in cell morphology and cell actin organization, cells were cultured on the NFL implants in growth medium for 7 days. Samples were fixed with 4% formalin and permeabilized with 0.2% Triton X-100 (Sigma, Germany) in PBS. Subsequently, the cells were stained with tetramethylrhodamine B isothiocyanate (TRITC)-labeled phalloidin (2.5 µg/ml, Sigma, Germany) to reveal the cytoskeletal organization of actin filaments and DAPI (2 µg/ml, Abcam, UK) to stain nuclei. Then, the samples were imaged by confocal microscopy (Leica SP8X, Germany) in which hybrid detectors collected the fluorescence signals from DAPI (405–480 nm) and phalloidin-TRITC (532–575 nm), which were given pseudo colours in the images. The cell orientations were colour coded and the orientation index was quantified using the Orientation J plugin (biomedical imaging group EPFL, Switzerland) in ImageJ software for three images per group.

2.8. Statistical analysis

Data are presented as mean ± standard deviation. Statistical analyses were conducted using SPSS (version 17, IBM Corporation, US). The Shapiro-Wilk test was used to test normality of the data distribution. The two-tailed student's *t*-test or one-way ANOVA with Tukey's post-hoc test was used for parametric data, while the Mann Whitney *U* test was used to evaluate the nonparametric fiber diameter data. A *P* value of 0.05 was used as a threshold for statistical significance. To determine the antibacterial efficiency, statistical analyses were performed on the log-transformed CFU data. **p* < .05; ***p* < .01; ****p* < .001.

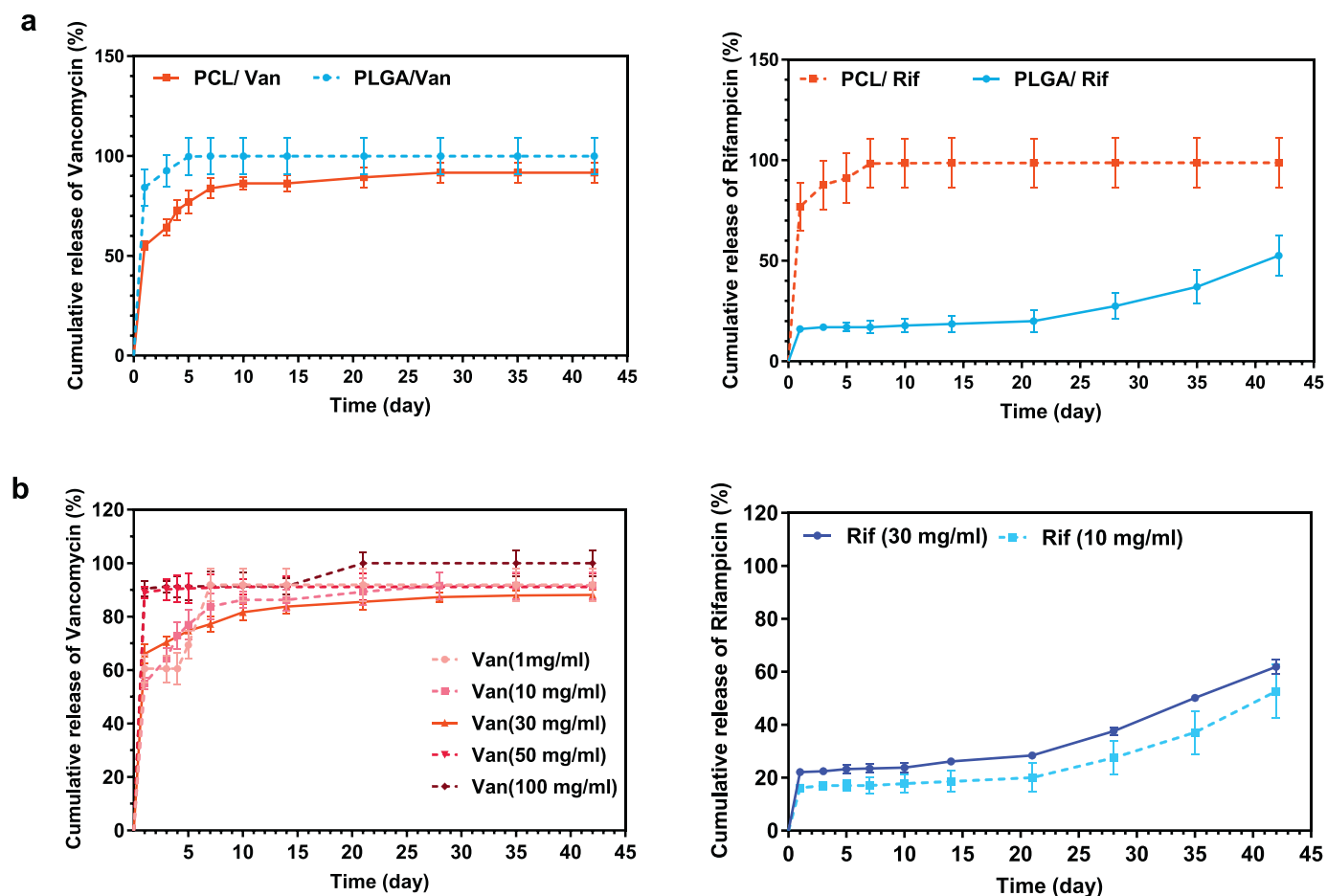


Fig. 2. *In vitro* antibiotics release profiles as determined by ultra-high performance liquid chromatography (UHPLC). (a) Cumulative release of Van and Rif loaded in PCL or PLGA nanofibers. (b) Cumulative release of Van and Rif from PCL/Van and PLGA/Rif nanofibers for different amounts of loaded drugs. Error bars depict mean \pm SD ($n = 3$).

3. Results

3.1. Nanofiber-filled lattice (NFL) structure

To optimize the sustained release kinetics of Rif and Van, a custom-built SES set-up was used to produce NFL implants composed of PCL and PLGA (Fig. 1, and Materials and methods). It was found that the Van and Rif release profiles could be tuned by selecting the appropriate drug-polymer combination. The combination of PCL/Van and PLGA/Rif resulted in a more sustained drug release than the PCL/Rif and PLGA/Van counterparts (Fig. 2a). In both polymer formulations, Van was released more rapidly than Rif, most likely due to the more hydrophilic character of Van compared to Rif. For these specific drug-polymer combinations, the drug release profiles depended on the drug content; the most gradual drug release over a period of 42 days was achieved by incorporation of 30 mg/ml Van in PCL and 30 mg/ml Rif in PLGA (Fig. 2b).

The nanofiber characteristics were analyzed before and after drug loading. Loading 30 mg/ml Van in PCL did not affect the fiber diameter (Fig. 3a, b), whereas loading 30 mg/ml Rif in PLGA significantly decreased the fiber diameter as compared to PLGA-alone nanofibers (Fig. 3a, c). The negligible effect of Van loading on the fiber diameter offers advantages, as it allows for a higher drug load, while the increased surface area-to-volume ratio preserves the interfacial adhesion strength between the nanofibers and the substrate [58,59].

Hydrophobicity of the NFL implants was measured via the initial water contact angle. This was similar for PCL and PLGA, and there were no significant changes after loading either Van or Rif (Fig. 3d). This

indicates that incorporation of these two drugs did not affect the overall hydrophobicity of PCL and PLGA fibers significantly, even though Van and Rif are known as large hydrophilic and hydrophobic molecules, respectively [60,61]. The results agree with other reports showing contact angles for PCL between 90° and 130° [38,62,63] and for PLGA between 110° and 130° [64–66].

The presence of Van and Rif in the nanofibers was confirmed by ATR-FTIR. The presence of Van in PCL/Van nanofibers was corroborated by the appearance of a peak at 3284 cm^{-1} (C–H) (Fig. 3e) and the presence of Rif in PLGA/Rif nanofibers by the appearance of a peak at 2880 cm^{-1} (C–H) (Fig. 3f). Although the peak assigned to PLGA at 2850–3000 cm^{-1} (due to CH vibration) [67] shows overlap with the peaks of Rif (due to CH₃, CH₂ and CH vibration) [68] in the FTIR spectrum of PLGA/Rif, the change in the intensity of the peak was able to show the successful incorporation of Rif in PLGA. The Van and Rif loading changed the mechanical properties of PCL and PLGA-electrospun nanofibers by decreasing the elongation of PCL and PLGA, respectively (Fig. 3g). Van loading reduced the stiffness of PCL, as measured via Young's modulus, while Rif loading increased the stiffness of PLGA (Fig. 3h).

3.2. Coating durability

To preserve the integrity of the nanofiber assembly after surgical implantation, the developed structures should withstand the mechanical shear forces posed upon it during handling and press-fit insertion into bone [69]. It was hypothesized that the development of nanofiber coatings into lattice surface structures could improve the coating

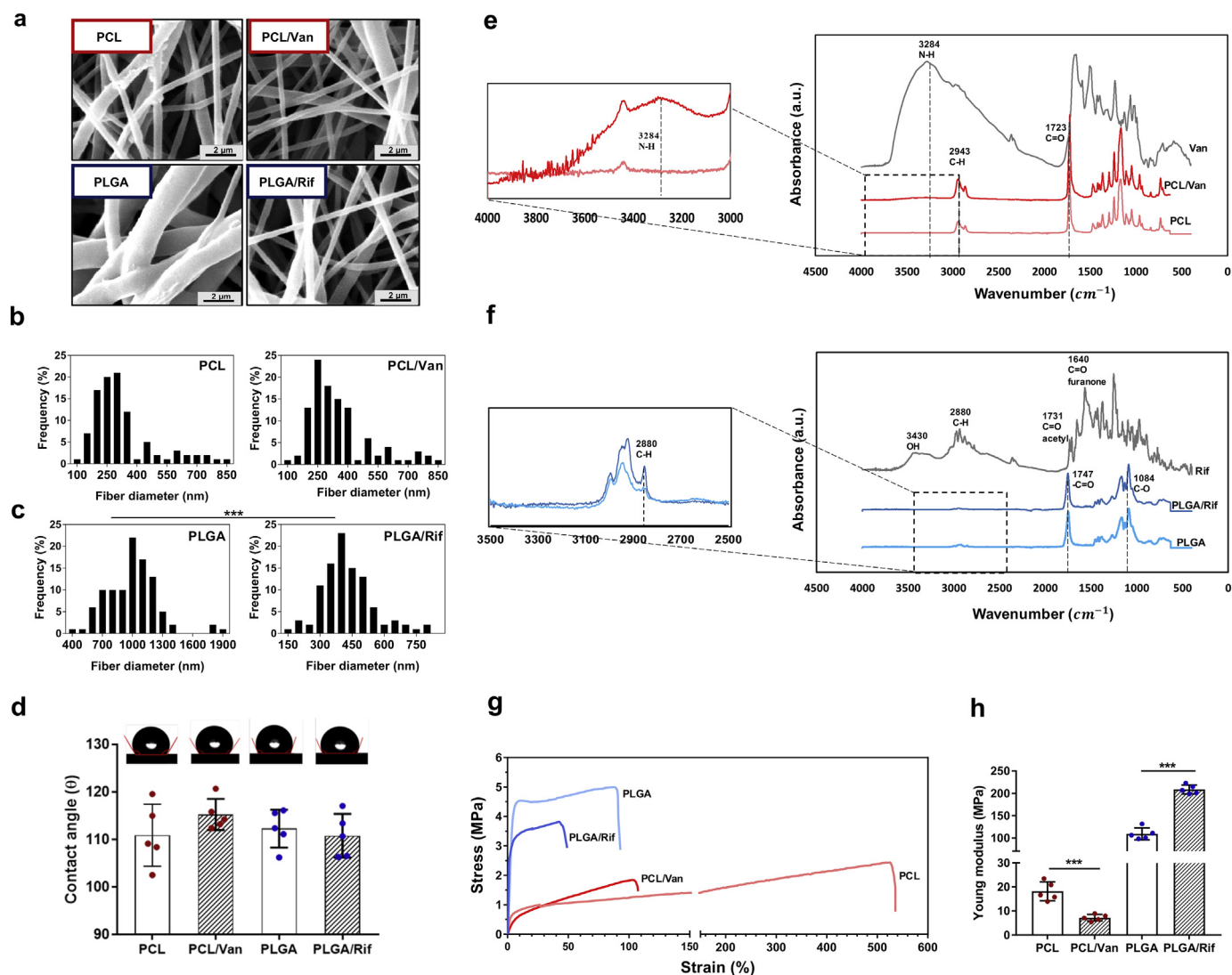


Fig. 3. Characterization of PCL, PLGA, PCL/Van and PLGA/Rif nanofiber structures. (a) SEM images of the nanofiber structure topographies. (b–c) Size distribution of the nanofiber diameters ($n = 100$ fibers/sample). (d) Water contact angles of the nanofiber structures ($n = 5$). (e) FTIR spectra of PCL and PCL/Van nanofiber structures. (f) FTIR spectra of PLGA and PLGA/Rif nanofiber structures. (g) Strain-stress curves of nanofiber structures ($n = 5$). (h) Young's modulus of nanofiber structures. Data are represented as the mean \pm SD.

durability in the NFL implants. Indeed, gross examination of implants after press-fit implantation in cadaveric bone and immediate removal showed delamination of the coating for nanofibers electrospun on solid Ti rods, whereas no damage was observed for the NFL implants (Fig. 4a). The lattice structure was particularly effective in preserving the nanofiber architecture when using multilayer nanofiber structures (Fig. 4b). Using fluorescently-labeled polymers for electrospinning, it was found that the multilayer assembly on the solid implant peeled back during bone insertion into the bone cavity space. In contrast, the nanofibers remained intact within the NFL implants (Fig. 4c). The results showed that the attachment strength between the nanofiber layer and Ti was improved in the NFL implants. Thus, the lattice structures in the NFL implants not only act as a drug depot for the nanofiber assembly, but also as protective areas to prevent mechanical delamination.

3.3. In vitro antibiotic release profile

To simultaneously address the possibilities of early and delayed infections, we aimed for combinatorial antibacterial efficacy supported by a customized release of Van and Rif. For this purpose, the random

blending of nanofibers containing Van or Rif was deemed inappropriate, as it would not yield a distinctive release profile of the respective drugs. Therefore, after a series of optimizations, two combinatorial drug-laden nanofiber structures, *i.e.* core-shell and bi-layered composites, were electrospun onto the implants to further tailor the drug release behavior. For the bi-layered structure, PCL/Van was assembled directly on the implant surface to form an inner layer, and PLGA/Rif was applied to form a surrounding outer layer, denoted as the bi-layered structure (Fig. 5a). The PLGA/Rif nanofibers were included as the outer layer in the bi-layered structures considering the better stiffness properties (Fig. 3g) beneficial for stem cell differentiation and proliferation [40,70], and the observation that the adhesion and differentiation of bone cells (osteoblasts) is superior on substrates with higher stiffness [71,72]. At the same time, using PLGA/Rif as an outer layer in the bi-layered structure is thought to prevent the burst release of Van and increase the longevity of the antibacterial effect. For the core-shell structure, a single layer was electrospun onto the implants using nanofibers composed of PCL/Van in the core and PLGA/Rif in the shell (Fig. 5b).

The two coating structures produced distinct drug release profiles (Fig. 5c and d). Quantitatively, more than 95% of Van and 80% of Rif

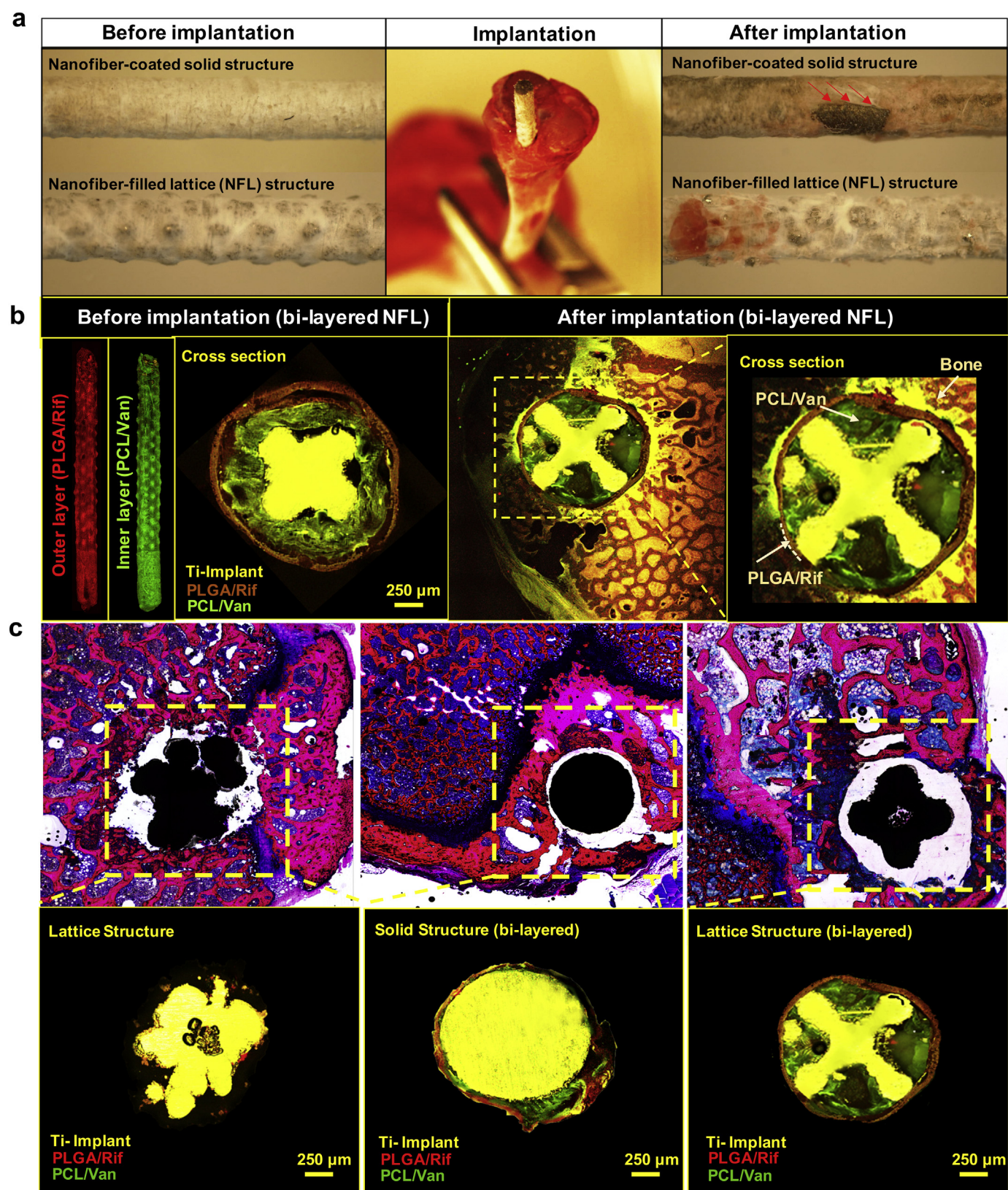


Fig. 4. *Ex vivo* bone implantation and integrity of electrospun nanofibers on solid and lattice structured implants. (a) Stereo microscope images, with arrows showing the fiber damaged during implantation. (b) Cross-sectional overview of lattice-structured implants with bi-layered nanofiber assembly before and after bone implantation as visualized by fluorescence microscopy. PCL/Van was labeled with FITC and PLGA/Rif was labeled with rhodamine B. (c) Methylene blue/basic fuchsin staining (top) and confocal imaging (bottom) of solid and lattice structure with and without bi-layered nanofiber assembly showing the implant positioning and coating integrity relative to the surrounding bone (pink). PCL/Van was labeled with FITC and PLGA/Rif was labeled with rhodamine B. Arrows highlight peeled-back coating after implantation. (For interpretation of the references to colour in this figure legend, the reader is referred to the web version of this article.)

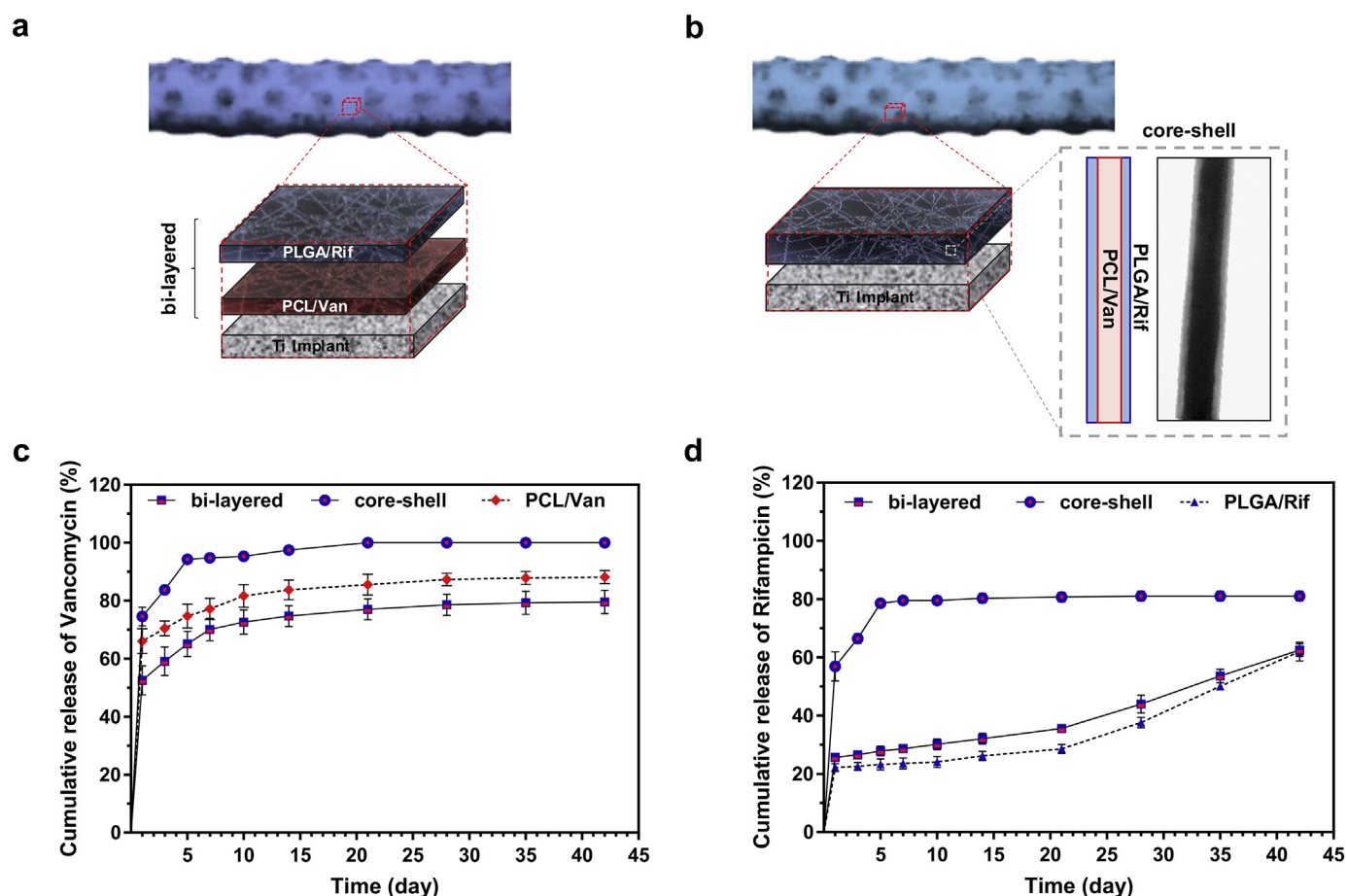


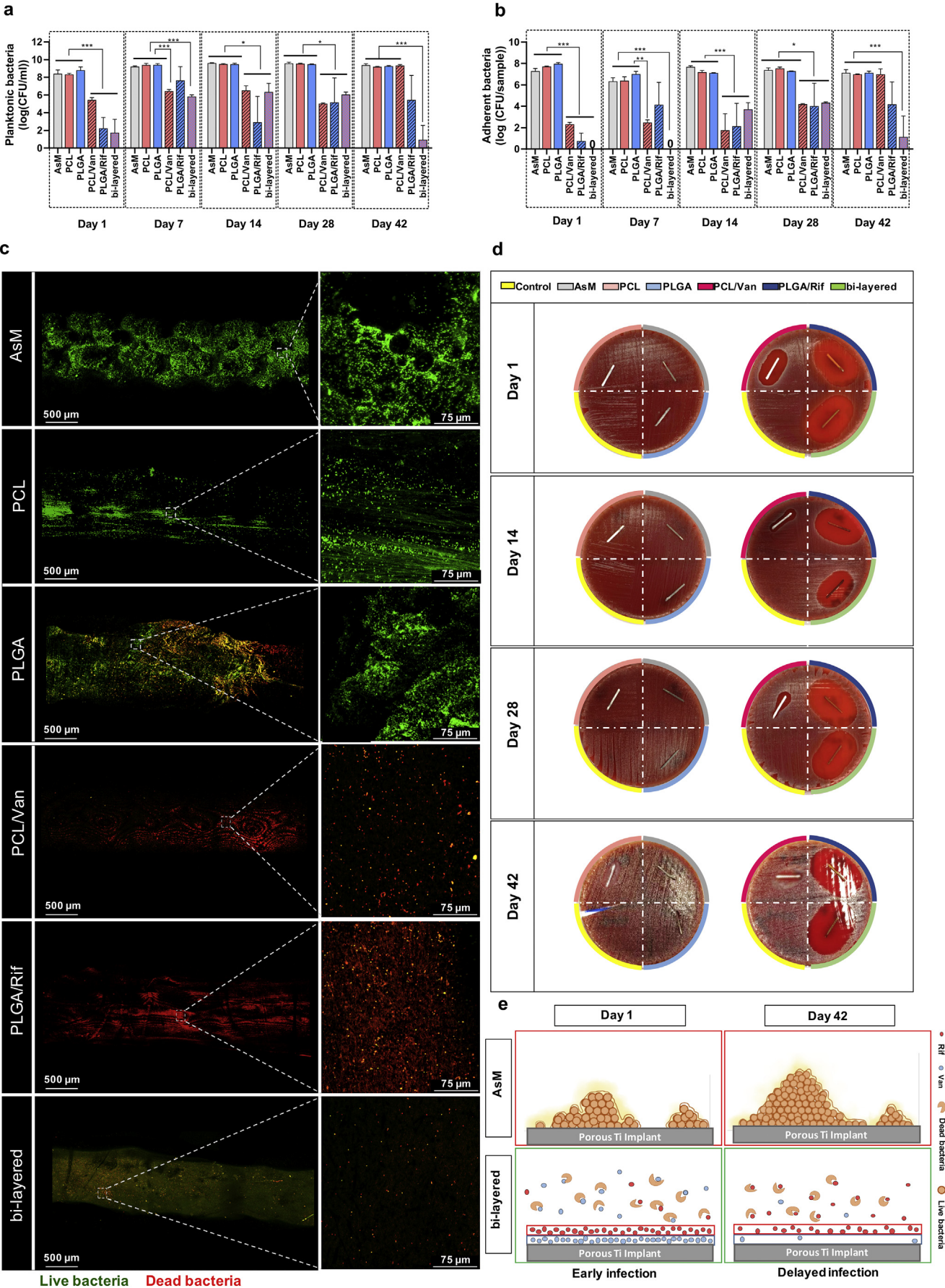
Fig. 5. Various assemblies of drug-laden NFL implants and *in vitro* antibiotics release profiles. (a) Schematic illustration of the bi-layered NFL, composed of PCL/Van as an inner layer and PLGA/Rif as an outer layer. (b) Schematic illustration of the core-shell NFL, composed of PCL/Van in the core and PLGA/Rif in the shell of nanofibers. TEM was used to verify the core-shell structure. (c-d) Cumulative Van (c) and Rif (d) release from three different NFL structures during 6 weeks as determined by UPLC. Data are presented as the mean \pm SD (n = 3).

were released within 7 days from the core-shell coating. Moreover, for the core-shell coating, most of the drug release occurred already in the first day, followed by additional release extending until day 14. This burst release profile produced by the core-shell structure may be due to either two phenomena: 1) mixture of the drug solution in the core and shell during electrospinning, and/or 2) imperfections in the core-shell structure leading to enhanced drug diffusion from the core to the shell [73]. In comparison, in the bi-layered structure, the application of PLGA/Rif as an outer layer led to more sustained Van release from the PCL/Van inner layer, without influencing the sustainability of the Rif release. Hence, only 50% of Van and 25% of Rif were released from the bi-layered coatings over a period of 14 days. Moreover, after an initial burst release of Van and Rif on the first day, a slower and more controlled drug release was seen extending over 42 days. In fact, only $62.52 \pm 1.79\%$ and $79.59 \pm 3.3\%$ of the total Rif and Van had been released during the evaluation period of 42 days, respectively. Based on the bi-phasic release seen for Rif, its sustained release can most likely be explained by a shift in drug-release mechanisms, that is, drug diffusion in the first 3 weeks, followed by both drug diffusion and PLGA degradation from thereon. Taken together, the bi-layered structure showed a superior sustained release behavior than the core-shell structure over a period of 6 weeks and was therefore tested for its durability upon implantation and its ability towards prolonged bacterial growth inhibition *in vitro*.

3.4. *In vitro* antibacterial behavior

The antimicrobial activity of the developed NFL implants against *Staphylococcus aureus* (*S. aureus*) was determined. All groups containing Van and/or Rif reduced both the planktonic and implant-adherent bacteria by at least 100-fold up to 28 days as compared to groups without antibiotics (Fig. 6a, b). The combinatorial delivery of Van and Rif from the bi-layered structure showed enhanced antibacterial effect as compared to the PCL/Van or PLGA/Rif single layers. Only the bi-layered implants demonstrated complete eradication of adherent bacteria, which was limited to the first week. In addition, a significant antibacterial effect towards planktonic and implant-adherent *S. aureus* was only seen at day 42 in the bi-layered implants. The enhanced antibacterial effect at day 42 was due to a synergistic bactericidal activity of Rif and Van against both planktonic and adherent *S. aureus*. In agreement, the bacterial live/dead assay demonstrated mostly non-viable bacteria in the Van and Rif groups after 24 h, whereas bacterial colonization was seen in groups without antibiotics (Fig. 6c). In the bi-layered group, not even dead bacteria were observed, suggesting a lack of initial bacterial adhesion after 24 h, and which confirms the previous quantification of surviving bacteria (Fig. 6b).

Antibacterial activity was also investigated by measuring the zone of inhibition (ZOI) around implants on contaminated agar plates. The Rif-loaded nanofibers showed the largest ZOI at all time points, with no decrease of the ZOI over time (Fig. 6d). In contrast, the ZOI in the PCL/Van group was maximal at day 1 and diminished at later time points. The ZOI method did not show a higher antibacterial effect of the bi-



(caption on next page)

Fig. 6. *In vitro* antimicrobial activity. (a–b) Quantification of CFU surviving 24 h incubation with antibiotics released from NFL implants at various timepoints, determined for both adherent (a) and planktonic-grown (b) bacteria. Data are represented as the mean \pm SD and (n = 3). (c) Bacterial live-dead staining 24 h after bacterial inoculation at day 1 (as in (a) and (b)). Live bacteria were stained with Cyto9 (green) and dead bacteria were stained with propidium iodide (red). (d) Bacterial growth inhibition at different time points. (e) Schematic representation of the proposed bactericidal activity of the bi-layered NFL implants against early and delayed infection. (For interpretation of the references to colour in this figure legend, the reader is referred to the web version of this article.)

layered structure as compared to the PLGA/Rif single layer, contrasting the observations made for planktonic bacterial killing (Fig. 6a, b). This could be due to the different antibiotic release or subsequent diffusion through the agar plates, underestimating the actual effects that would occur in an aqueous environment or at the site of infection [74,75].

Together, these results suggest a superiority of the bi-layered structure in bacterial killing as compared to single layer structures, covering not only immediate, but also extended antibacterial effectiveness up to 42 days. The extended antibacterial response most likely stems from the bi-phasic release observed for Rif, with secondary rapid release of Rif starting after approximately 20 days (Fig. 5d and 6e).

3.5. *In vitro* cell viability, proliferation, and morphology

Orthopedic implant surfaces should support the adhesion and overgrowth by bone cells. Using a qualitative live-dead assay, it was found that MC3T3 osteoblast precursor cells adhered and spread homogeneously on all NFL implants, with full coverage observed after 14 days (Fig. 7a). The low percentage of dead cells indicated no adverse effect of the NFL implant on cell viability, irrespective of the drug loading (Fig. 7b). The cytocompatibility of the different structures was confirmed with the quantitative Alamar blue assay, showing a steadily increasing total metabolic activity over a period of 14 days (Fig. 7c). At day 14, a significantly lower metabolic activity was seen for the non-coated and PCL samples as compared to all other groups, indicating that coating improves osteoblast proliferation or metabolic activity (Fig. 7c). When comparing the actin organization in cells seeded onto bi-layered and non-coated implants, the bi-layered group demonstrated a more highly organized orientation (Fig. 7d) and an actin orientation index of 4.6 times higher than non-coated implants (Fig. 7e and f). This finding agrees with other reports showing that actin stress fibers are extended preferentially in line with the nanofiber orientation, and which follows the premise that cell filopodia tend to orient along the direction of the features and determine cytoskeleton orientation [76,77]. The excellent cytocompatibility of the NFL implants could therefore be in part explained by its extracellular matrix like-texture and the effect on cell contact guidance, which could modulate cell morphology, integrin expression, and spreading and differentiation to promote implant-bone integration [78].

4. Discussion

In light of the current clinical challenges to prevent IAI, electrospinning was employed to develop a novel coating structure with combinatorial antibacterial activity. Using Van and Rif as model drugs, we found that the deposition of a bi-layered nanofiber composition onto a microporous lattice structure was a feasible approach to 1) extend the period in which drug concentrations are high enough to be effective, showing for the first-time antibacterial efficacy *in vitro* for 6 weeks, and 2) improve the resistance to coating delamination during surgical implantation without the need of an additional heat or chemical treatment step.

A major drawback of currently approved local antibiotic delivery systems in orthopedic practice, such as poly(methyl methacrylate) spacers or beads, is that they have been optimized to release a single antibiotic [11], whereas clinically, combinatorial drug delivery has proven to be more effective for bacterial eradication [21]. Rif was chosen as the first antibacterial drug considering its high effectiveness to prevent and eliminate *staphylococcal* IAI [24,79,80]. Importantly, the

use of Rif alone is a double-edge sword because Rif monotherapy yields a high risk of resistance development, which hampers its widespread use as prophylactic agent for IAI [25]. Moreover, current evidence indicates that Rif's bactericidal effects are enhanced when combined with other antibiotics [21], opting this to be further explored in a local delivery system. We selected Van as a companion drug for Rif because it is the recommended antibiotic for MRSA, a common and difficult-to-treat pathogen in IAI [81]. Secondly, it was hypothesized that, due to their distinct physical properties, the combination of Rif and Van in the hydrophobic PLGA/PCL bi-layered structure coating would lead to more readily tunable and/or sustainable release profiles. Using this approach, we demonstrated an enhanced antibacterial effect of the bi-layered structure as compared to the PCL/Van or PLGA/Rif single layers at both early and delayed time points. Moreover, after 42 days, a synergistic bactericidal activity of the [PCL/Van]/[PLGA/Rif] bi-layered structure was found against planktonic and implant-adherent *S. aureus*. This finding strengthens the literature that has hinted towards a synergistic bactericidal effect of Van and Rif *in vitro* [82,83] and *in vivo* [84,85]. Together, this shows that electrospun bi-layered composites could be a strategy to achieve local inhibitory antibiotic concentrations over a longer time, which in turn reduces the chance of antibiotics resistance. In the future, other promising drug combination for IAI prevention could be investigated in the bi-layered coating, including antimicrobial peptides [86] or immunomodulatory agents [87,88].

Since the available antibacterial hydrogel coatings rapidly resorb and only protect against early infections [89,90], several attempts have been made to use electrospun coatings as an antibiotic delivery system to prevent IAI [35,44,91]. However, none of these reports present a sustained antibacterial strategy that could cover both an early and delayed onset of infection. In the design of an improved composite coating, we considered several important parameters such as the i) type of polymer, ii) drug physiochemical properties, iii) drug-polymer interaction and iv) electrospinning processing parameters [26]. As depicted in Fig. 8, the resulting [PCL/Van]/[PLGA/Rif] bi-layered composite showed a bi-phasic release profile with both early and delayed antibacterial action (Fig. 8c), which single-layer coatings did not (Fig. 8a, b). Despite the high *S. aureus* inoculation dose, the developed [PCL/Van]/[PLGA/Rif] bi-layered composite protected fully against biofilm formation during the first week (Fig. 6b). Based on the "race for the surface" theory [92], inhibition of bacterial adherence during this critical time span will allow early tissue formation which further reduces the likelihood of implant infection (Fig. 8c). Moreover, due to the extended release profile associated with the bi-layered nanofiber composite, an antibacterial action was sustained for at least 6 weeks *in vitro*.

The current coating can be considered highly tunable, as changes in type of polymer (PCL and PLGA), antibiotics (Van and Rif) and electrospun structures (simple and core-shell nanofibers), all provide opportunities to tailor the drug release profile to combat early and/or delay IAI. We propose that the specific drug-polymer interaction, in conjunction with the bi-layered composite, underlies the observed extended antibacterial effectiveness (Fig. 8). These two parameters are critical for extending the period during which inhibitory drug concentrations are sustained, collectively resulting in a superior system than the reported use of single nanofiber or basic co-spinning strategies [44]. First, the drug release from polymeric nanofibers is attributed to the drug diffusion and degradation rate, as well as the chemical structure of the chosen polymers [28]. In the case of polymer chemical composition, the release rate of hydrophobic polymers, such as PCL and PLGA, can range from days to months, and is determined by a

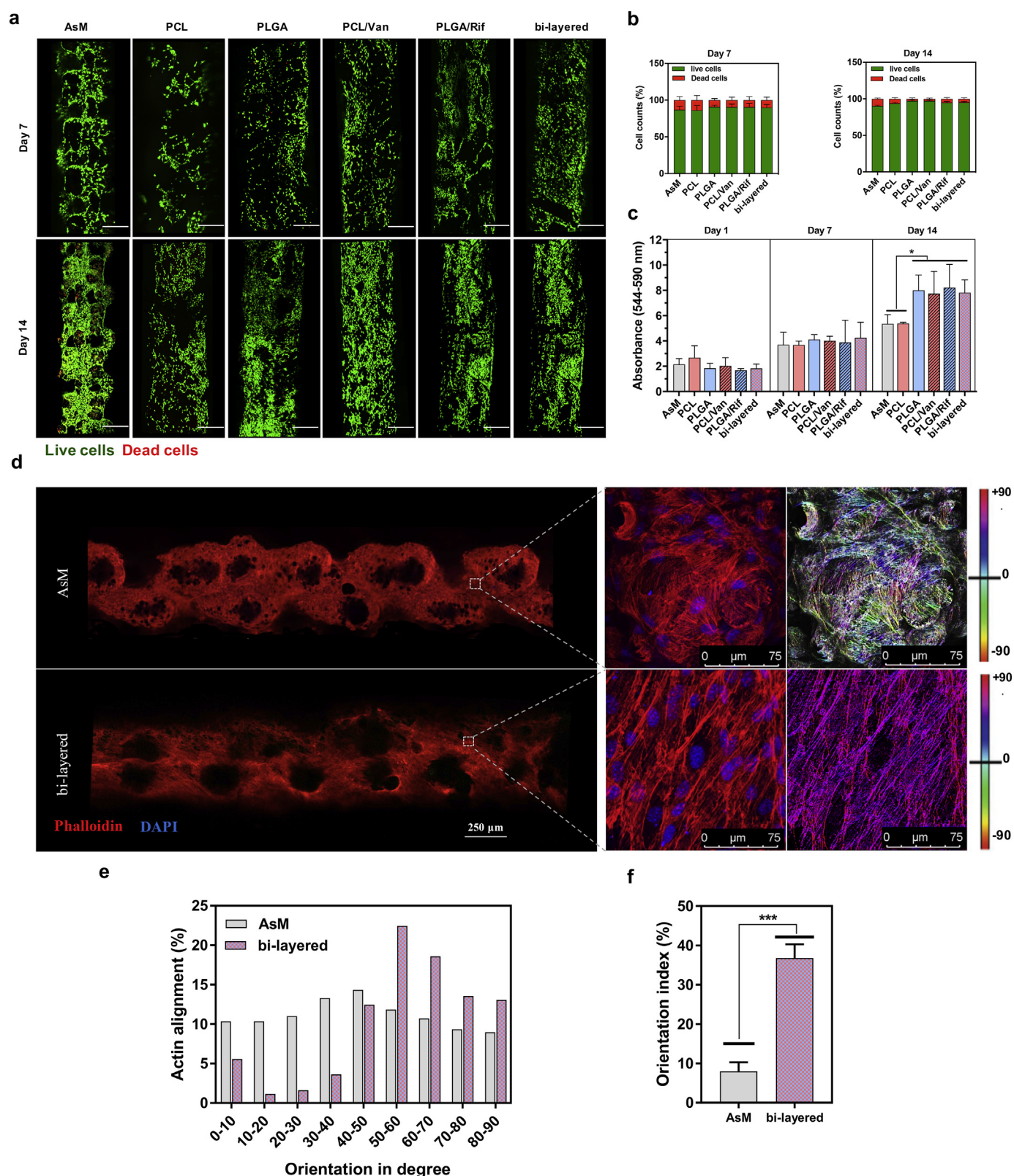


Fig. 7. Cytocompatibility of the drug-laden NFL implants. (a) Live-dead staining performed on pre-osteoblast cells cultured on the NFL implants (scalebar = 500 μ m). (b) Quantification of live-dead staining after pre-osteoblast cell culture on NFL implants. (c) Alamar blue quantification of metabolic activity after pre-osteoblast cell culture on NFL implants. (d) Phalloidin (actin)/DAPI (DNA) staining of bi-layered NFL structured and empty latticed structure implants with pre-osteoblast cells (left). Images were also colour coded based on the actin orientation (right). (e) Degree of cellular actin alignment occurring on bi-layered NFL structured and empty lattice structured implants. (f) Orientation index of cellular actin. Data are presented as the mean \pm SD ($n = 3$). (For interpretation of the references to colour in this figure legend, the reader is referred to the web version of this article.)

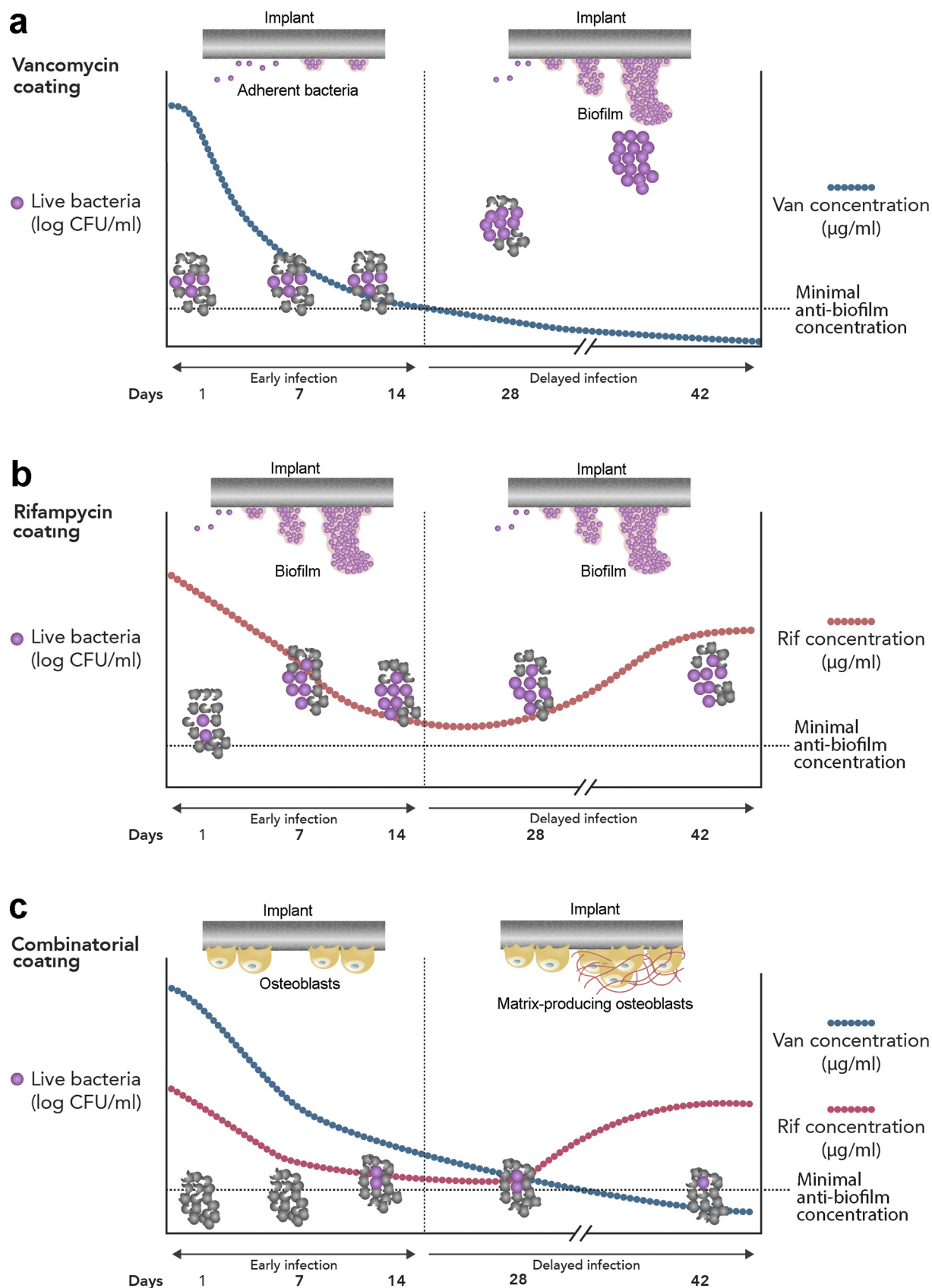


Fig. 8. Schematic illustration of the bactericidal effect and drug release of Vancomycin-laden (a), Rifampicin-laden (b), and Vancomycin/Rifampicin bi-layered (c) NFL implants with respect to early and delayed onset infection. The schematic is based on the drug release curves shown in Figs. 2 and 5, and the CFU data shown in Fig. 6b.

combination of drug diffusion processes, as well as polymer degradation mechanisms [43]. We showed that the combination of a hydrophobic polymer (PCL) with a hydrophilic antibiotic (Van), and another hydrophobic polymer (PLGA) with a hydrophobic antibiotic (Rif) enabled us to tune their release behavior in a wide timespan. Accordingly, PCL, as a semi-crystalline polymer, can be used for sustained release of hydrophilic drugs, such as Van due to the slower rate of water diffusion into the biomaterial [44,45], whereas the controlled release of Rif from PLGA is explained by the high molecular weight of Rif and the stronger hydrophobic – hydrophobic interactions between PLGA and Rif [18]. Second, the drug loading plays a key role in the drug dispersion and release behavior [93]. On the one hand, a minimal amount of Van is needed for its sustained antibacterial efficiency. On the other hand, an increase in Van concentration creates an acidic environment and causes PCL swelling, followed by water diffusion into the matrix [94]. This in turn results in a higher degradability of PCL and a burst release of Van (Fig. 2b). Hence, an intermediate Van loading (30 mg/ml) was found to be optimal in the current study. In the case of Rif, higher concentrations changed the fiber shape during the electrospinning process and were therefore avoided (Fig. 2). Third, the combinatorial effects of Van and Rif were further modulated by applying either a bi-layered or core-shell composite structure (Fig. 5a). In the bi-layered structure, using PLGA/Rif as an outer layer is thought to prevent the burst release of Van and increase the longevity of the antibacterial effect (Fig. 5b). In core-shell structures, however, mixing of the core-shell drug solution during electrospinning and also defects in the core-shell structure led to diffusion of drugs from the core to the shell. These can result in a burst release of drugs encapsulated in the core [95]. It can be concluded that neither the use of different polymers, nor converging different additive manufacturing techniques could resolve the core-shell structure imperfections issue and it is necessary to perform further research on different polymers to find an optimal approach.

In the cadaveric implantation model, we showed proof-of-concept that the coating on the NFL implants could resist press-fit insertion, while preserving the developed multi-layer coating architecture. We hypothesized that this NFL implant design was needed, as clinical experience teaches us that the typical forces exerted on the implant surface during press-fit implantation are excessive, even causing failure the metal or bone [7,96], and which would certainly remove any coating. In order to produce a durable coating, heat treatment of electrospun PCL coatings has previously been proposed [44]. As a limitation of this method, loss of activity of heat-sensitive antibiotics cannot be excluded [97], and moreover, this approach is not suitable for protein incorporation as they are prone to denaturation at increased temperature. There are two mechanisms by which the NFL implant design creates a durable coating, without needing heat or chemical treatment. First, the presence of a micro-porous surface is thought to enhance the mechanical interlock between polymers and metals, as surface topography is a major factor providing adhesion strength [98]. This could explain the higher resistance of the NFL coating to delamination as we observed. Second, the NFL provides ‘protective’ areas for bulk material of drug-loaded polymer, acting as a long-term drug depot. The latter characteristic is particularly important when using roughened implant surfaces, as they will be exposed to even higher shear fixation strengths than smooth surfaces [99]. Moreover, this is important to preserve the multi-layer design as used here. The current NFL implant design could be applied as an outer layer on implants, but is also compatible for entirely porous implants, including additively-manufactured orthopedic implants designed to match the mechanical properties of native bone [100] or new classes of porous metal bone substitutes [101,102]. In addition to the coating durability, a long-term bio-stability is another important coating property. In the current study, we found that drug elution was still ongoing after 42 days, at which point approximately 40% and 20% of the total Rif and Van, respectively, was still retained in the coating. The total bio-degradation time of the developed structures was not quantified, as it has already been reported numerously that

similar PCL or PLGA nanofiber structures have bio-degradation times of several months [103,104]. In agreement, our preliminary results show that the developed structures have at least 28 days bio-stable and drug-eluting properties *in vivo* (not shown). As part of these *in vivo* studies, it is currently investigated if this also renders the implants with the ability to prevent late orthopedic infections.

5. Conclusion

A bi-layered electrospun coating was applied onto 3D-printed Ti implants with a lattice geometry with the goal of obtaining a combinatorial and sustainable antibiotics release profile to surpass the acute postoperative period. The specific drug-polymer interaction, in combination with the bi-layer structure, in this approach was found to be critical for extending the inhibitory drug concentrations, showing for the first-time antibacterial efficacy for more than 6 weeks. The co-delivery of Rif and Van from the bi-layered structure demonstrated a combinatorial effect in terms of bactericidal activity. The nanofiber-filled lattice strategy that was employed resulted in a high durability of the coatings after surgical implantation. The current technology can be used to develop tunable coatings for various metallic implantable devices when drug release is required over a period of weeks, including but not limited to the delivery of multiple antimicrobial agents. In the future, the technology can be extended towards multifunctional coatings for sequential release of antibacterial as well as osteoinductive agents to render the orthopedic implants with a complete performance.

Acknowledgments

The research for this paper was financially supported by the PROSPEROS project, funded by the Interreg VA Flanders – The Netherlands program, CCI grant no. 2014TC16RFCB046. Also, the collaboration project is co-funded by the PPP Allowance made available by Health~Holland (LSHM18026), Top Sector Life Sciences & Health, to stimulate public-private partnerships.

References

- [1] R. Agarwal, A.J. Garcia, Biomaterial strategies for engineering implants for enhanced osseointegration and bone repair, *Adv. Drug Deliv. Rev.* 94 (2015) 53–62.
- [2] R.J. Ferguson, A.J.R. Palmer, A. Taylor, M.L. Porter, H. Malchau, S. Glyn-Jones, Hip replacement, *Lancet* 392 (2018) 1662–1671.
- [3] A.J. Price, A. Alvand, A. Troelsen, J.N. Katz, G. Hooper, A. Gray, A. Carr, D. Beard, Knee replacement, *Lancet* 392 (2018) 1672–1682.
- [4] T. Sorsa, D. Giesemann, N.B. Arweiler, M. Hernández, A quantitative point-of-care test for periodontal and dental peri-implant diseases, *Nat. Rev. Dis. Prim.* 3 (2017) 17069.
- [5] C.R. Arciola, D. Campoccia, L. Montanaro, Implant infections: adhesion, biofilm formation and immune evasion, *Nat. Rev. Microbiol.* 16 (2018) 397.
- [6] X. Jin, Y.H. Xiong, X.Y. Zhang, R. Wang, Y. Xing, S. Duan, D. Chen, W. Tian, F.J. Xu, Self-adaptive antibacterial porous implants with sustainable responses for infected bone defect therapy, *Adv. Funct. Mater.* 29 (2019) 1807915.
- [7] N.J. Hickok, I.M. Shapiro, Immobilized antibiotics to prevent orthopaedic implant infections, *Adv. Drug Deliv. Rev.* 64 (2012) 1165–1176.
- [8] P.S. Stewart, J.W. Costerton, Antibiotic resistance of bacteria in biofilms, *Lancet* 358 (2001) 135–138.
- [9] R.L. Barrack, J. Sawhney, J. Hsu, R.H. Cofield, Cost analysis of revision total hip arthroplasty. A 5-year followup study, *Clin. Orthop. Relat. Res.* (1999) 175–178.
- [10] A. Luu, F. Syed, G. Raman, A. Bhalla, E. Muldoon, S. Hadley, E. Smith, M. Rao, Two-stage arthroplasty for prosthetic joint infection: a systematic review of acute kidney injury, systemic toxicity and infection control, *J. Arthroplast.* 28 (2013) 1490–1498. e1491.
- [11] O.S. Kluin, H.C. van der Mei, H.J. Busscher, D. Neut, Biodegradable vs non-biodegradable antibiotic delivery devices in the treatment of osteomyelitis, *Expert Opin. Drug Deliv.* 10 (2013) 341–351.
- [12] J. Van Der Stok, D. Lozano, Y.C. Chai, S. Amin Yavari, A.P. Bastidas Coral, J.A. Verhaar, E. Gómez-Barrena, J. Schrooten, H. Jahr, A.A. Zadpoor, Osteostatin-coated porous titanium can improve early bone regeneration of cortical bone defects in rats, *Tissue Eng. A* 21 (2015) 1495–1506.
- [13] D. King, S. McGinty, Assessing the potential of mathematical modelling in designing drug-releasing orthopaedic implants, *J. Control. Release* 239 (2016) 49–61.
- [14] S. Amin Yavari, M. Croes, B. Akhavan, F. Jahanmard, C.C. Eigenhuis, S. Dadbakhsh, H.C. Vogely, M.M. Bilek, A.C. Fluit, C.H.E. Boel, B.C.H. van der Wal,

- T. Vermonden, H. Weinans, A.A. Zadpoor, Layer by layer coating for bio-functionalization of additively manufactured meta-biomaterials, *Addit. Manuf.* 32 (2020) 100991.
- [15] R. Devine, P. Singha, H. Handa, Versatile biomimetic medical device surface: hydrophobic coated, nitric oxide-releasing polymer for antimicrobial and hemocompatible applications, *Biomater. Sci.* 7 (2019) 3438–3449.
- [16] S. Bakhshandeh, Z. Gorgin Karaji, K. Lietaert, A.C. Fluit, C.H.E. Boel, H.C. Vogely, T. Vermonden, W.E. Hennink, A.A. Zadpoor, S. Amin Yavari, Simultaneous delivery of multiple antibacterial agents from additively manufactured porous biomaterials to fully eradicate planktonic and adherent *Staphylococcus aureus*, *ACS Appl. Mater. Interfaces* 9 (2017) 25691–25699.
- [17] B. Akhavan, S. Bakhshandeh, H. Najafi-Ashtiani, A.C. Fluit, E. Boel, C. Vogely, B.C. Van Der Wal, A.A. Zadpoor, H. Weinans, W.E. Hennink, Direct covalent attachment of silver nanoparticles on radical-rich plasma polymer films for antibacterial applications, *J. Mater. Chem. B* 6 (2018) 5845–5853.
- [18] S.E. Gilchrist, D. Lange, K. Letchford, H. Bach, L. Fazli, H.M. Burt, Fusidic acid and rifampicin co-loaded PLGA nanofibers for the prevention of orthopedic implant associated infections, *J. Control. Release* 170 (2013) 64–73.
- [19] A.F. Widmer, New Developments in Diagnosis and Treatment of Infection in Orthopedic Implants, The University of Chicago Press, 2001.
- [20] L. Hall-Stoodley, J.W. Costerton, P. Stoodley, Bacterial biofilms: from the natural environment to infectious diseases, *Nat. Rev. Microbiol.* 2 (2004) 95.
- [21] J. Lora-Tamayo, O. Murillo, J.A. Iribarren, A. Soriano, M. Sánchez-Somolinos, J.M. Baraia-Etxaburu, A. Rico, J. Palomino, D. Rodríguez-Pardo, J.P. Horcajada, A large multicenter study of methicillin-susceptible and methicillin-resistant *Staphylococcus aureus* prosthetic joint infections managed with implant retention, *Clin. Infect. Dis.* 56 (2012) 182–194.
- [22] D. Teterycz, T. Ferry, D. Lew, R. Stern, M. Assal, P. Hoffmeyer, L. Bernard, I. Uçkay, Outcome of orthopedic implant infections due to different staphylococci, *Int. J. Infect. Dis.* 14 (2010) e913–e918.
- [23] C. Liu, A. Bayer, S.E. Cosgrove, R.S. Daum, S.K. Fridkin, R.J. Gorwitz, S.L. Kaplan, A.W. Karchmer, D.P. Levine, B.E. Murray, Clinical practice guidelines by the Infectious Diseases Society of America for the treatment of methicillin-resistant *Staphylococcus aureus* infections in adults and children, *Clin. Infect. Dis.* 52 (2011) e18–e55.
- [24] W. Zimmerli, A.F. Widmer, M. Blatter, R. Frei, P.E. Ochsen, Role of rifampin for treatment of orthopedic implant-related staphylococcal infections: a randomized controlled trial, *JAMA* 279 (1998) 1537–1541.
- [25] D.-M. Zavasky, M.A. Sande, Reconsideration of rifampin: a unique drug for a unique infection, *JAMA* 279 (1998) 1575–1577.
- [26] E.M. Pritchard, T. Valentin, B. Panilaitis, F. Omenetto, D.L. Kaplan, Antibiotic-releasing silk biomaterials for infection prevention and treatment, *Adv. Funct. Mater.* 23 (2013) 854–861.
- [27] C.L. Romanò, H. Tsuchiya, I. Morelli, A.G. Battaglia, L. Drago, Antibacterial coating of implants: are we missing something? *Bone Joint Res.* 8 (2019) 199–206.
- [28] K.Y. Lee, L. Jeong, Y.O. Kang, S.J. Lee, W.H. Park, Electrospinning of polysaccharides for regenerative medicine, *Adv. Drug Deliv. Rev.* 61 (2009) 1020–1032.
- [29] H.S. Yoo, T.G. Kim, T.G. Park, Surface-functionalized electrospun nanofibers for tissue engineering and drug delivery, *Adv. Drug Deliv. Rev.* 61 (2009) 1033–1042.
- [30] Y. Liu, L. Deng, C. Zhang, F. Feng, H. Zhang, Tunable physical properties of ethylcellulose/gelatin composite nanofibers by electrospinning, *J. Agric. Food Chem.* 66 (2018) 1907–1915.
- [31] F. Topuz, T. Uyar, Electrospinning of gelatin with tunable fiber morphology from round to flat/ribbon, *Mater. Sci. Eng. C* 80 (2017) 371–378.
- [32] Z. Liu, J.-h. Zhao, P. Liu, J.-h. He, Tunable surface morphology of electrospun PMMA fiber using binary solvent, *Appl. Surf. Sci.* 364 (2016) 516–521.
- [33] R.J. Stoddard, A.L. Steger, A.K. Blakney, K.A. Woodrow, In pursuit of functional electrospun materials for clinical applications in humans, *Ther. Deliv.* 7 (2016) 387–409.
- [34] S. Zupancic, L. Casula, T. Rijavec, A. Lapanje, M. Lustrik, A.M. Fadda, P. Kocbek, J. Kristl, Sustained release of antimicrobials from double-layer nanofiber mats for local treatment of periodontal disease, evaluated using a new micro flow-through apparatus, *J. Control. Release* 316 (2019) 223–235.
- [35] L.-I. Li, L.-m. Wang, Y. Xu, L.-x. Lv, Preparation of gentamicin-loaded electrospun coating on titanium implants and a study of their properties in vitro, *Arch. Orthop. Trauma Surg.* 132 (2012) 897–903.
- [36] A.R. Tsiapla, V. Karagkiozaki, F. Pappa, V. Bakola, T. Choli-Papadopolou, I. Moutsios, E. Pavlidou, A. Laskarakis, S. Logothetidis, Drug delivery nanoplateform for orthopaedic-associated infections, *Mater. Today Proc.* 4 (2017) 6880–6888.
- [37] L. Zhang, J. Yan, Z. Yin, C. Tang, Y. Guo, D. Li, B. Wei, Y. Xu, Q. Gu, L. Wang, Electrospun vancomycin-loaded coating on titanium implants for the prevention of implant-associated infections, *Int. J. Nanomedicine* 9 (2014) 3027.
- [38] S.H. Ku, C.B. Park, Human endothelial cell growth on mussel-inspired nanofiber scaffold for vascular tissue engineering, *Biomaterials* 31 (2010) 9431–9437.
- [39] J. Wu, Z. Zhang, J. Gu, W. Zhou, X. Liang, G. Zhou, C.C. Han, S. Xu, Y. Liu, Mechanism of a long-term controlled drug release system based on simple blended electrospun fibers, *J. Control. Release* 320 (2020) 337–346.
- [40] X. Liu, Y. Yang, D.-G. Yu, M.-J. Zhu, M. Zhao, G.R. Williams, Tunable zero-order drug delivery systems created by modified triaxial electrospinning, *Chem. Eng. J.* 356 (2019) 886–894.
- [41] Y. Yang, W. Li, D.-G. Yu, G. Wang, G.R. Williams, Z. Zhang, Tunable drug release from nanofibers coated with blank cellulose acetate layers fabricated using triaxial electrospinning, *Carbohydr. Polym.* 203 (2019) 228–237.
- [42] M. Bay Stie, M. Corezzi, A.D. Juncos Bombin, F. Ajallouiean, E. Attrill, S. Pagliara, J. Jacobsen, I.S. Chronakis, H. Mørck Nielsen, V. Foderà, Waterborne electrospinning of alpha-lactalbumin generates tunable and biocompatible nanofibers for drug delivery, *ACS Appl. Nano Mater.* 3 (2) (2020) 1910–1921.
- [43] A. Kiran, T. Kumar, R. Sanghavi, M. Doble, S. Ramakrishna, Antibacterial and bioactive surface modifications of titanium implants by PCL/TiO₂ nanocomposite coatings, *Nanomaterials* 8 (2018) 860.
- [44] A.G. Ashbaugh, X. Jiang, J. Zheng, A.S. Tsai, W.-S. Kim, J.M. Thompson, R.J. Miller, J.H. Shahbazian, Y. Wang, C.A. Dillen, Polymeric nanofiber coating with tunable combinatorial antibiotic delivery prevents biofilm-associated infection in vivo, *Proc. Natl. Acad. Sci.* 201613722 (2016).
- [45] R. Boia, P.A.N. Dias, J.M. Martins, C. Galindo-Romero, I.D. Aires, M. Vidal-Sanz, M. Agudo-Barriuso, H.C. de Sousa, A.F. Ambrósio, M.E.M. Braga, A.R. Santiago, Porous poly(ϵ -caprolactone) implants: a novel strategy for efficient intraocular drug delivery, *J. Control. Release* 316 (2019) 331–348.
- [46] B.B. Mandal, A. Grinberg, E. Seok Gil, B. Panilaitis, D.L. Kaplan, High-strength silk protein scaffolds for bone repair, *Proc. Natl. Acad. Sci.* 109 (2012) 7699–7704.
- [47] X. Feng, J. Li, X. Zhang, T. Liu, J. Ding, X. Chen, Electrospun polymer micro/nanofibers as pharmaceutical repositories for healthcare, *J. Control. Release* 302 (2019) 19–41.
- [48] O.W. Bastian, M. Croes, J. Alblas, L. Koenderman, L.P.H. Leenen, T.J. Blokhuis, Neutrophils inhibit synthesis of mineralized extracellular matrix by human bone marrow-derived stromal cells in vitro, *Front. Immunol.* 9 (2018) 945.
- [49] A.R. D'Amato, N.J. Schaub, J.M. Cardenas, E. Franz, D. Rende, A.M. Ziemba, R.J. Gilbert, Evaluation of procedures to quantify solvent retention in electrospun fibers and facilitate solvent removal, *Fibers Polym.* 18 (2017) 483–492.
- [50] K. Ghosal, S. Thomas, N. Kalarikkal, A. Gnanamani, Collagen coated electrospun polycaprolactone (PCL) with titanium dioxide (TiO₂) from an environmentally benign solvent: preliminary physico-chemical studies for skin substitute, *J. Polym. Res.* 21 (2014) 410.
- [51] D.N. Heo, H.-J. Kim, Y.J. Lee, M. Heo, S.J. Lee, D. Lee, S.H. Do, S.H. Lee, I.K. Kwon, Flexible and highly biocompatible nanofiber-based electrodes for neural surface interfacing, *ACS Nano* 11 (2017) 2961–2971.
- [52] J. Jin, P. Hassanzadeh, G. Perotto, W. Sun, M.A. Brenckle, D. Kaplan, F.G. Omenetto, M. Rolandi, A biomimetic composite from solution self-assembly of chitin nanofibers in a silk fibroin matrix, *Adv. Mater.* 25 (2013) 4482–4487.
- [53] M. Croes, S. Bakhshandeh, I.A.J. van Hengel, K. Lietaert, K.P.M. van Kessel, B. Pouran, B.C.H. van der Wal, H.C. Vogely, W. Van Heck, A.C. Fluit, C.H.E. Boel, J. Alblas, A.A. Zadpoor, H. Weinans, S. Amin Yavari, Antibacterial and immunogenic behavior of silver coatings on additively manufactured porous titanium, *Acta Biomater.* 81 (2018) 315–327.
- [54] H. Yuan, H. Fernandes, P. Habibovic, J. de Boer, A.M. Barradas, A. de Ruiter, W.R. Walsh, C.A. van Blitterswijk, J.D. de Bruijn, Osteoinductive ceramics as a synthetic alternative to autologous bone grafting, *Proc. Natl. Acad. Sci.* 107 (2010) 13614–13619.
- [55] M. Croes, H. de Visser, B.P. Meij, K. Lietart, B.C.H. van der Wal, H.C. Vogely, A.C. Fluit, C.H.E. Boel, J. Alblas, H. Weinans, S. Amin Yavari, Data on a rat infection model to assess porous titanium implant coatings, *Data Brief* 21 (2018) 1642–1648.
- [56] T.A.M. Valente, D.M. Silva, P.S. Gomes, M.H. Fernandes, J.D. Santos, V. Sencadas, Effect of sterilization methods on electrospun poly(lactic acid) (PLA) Fiber alignment for biomedical applications, *ACS Appl. Mater. Interfaces* 8 (2016) 3241–3249.
- [57] C.F. Redigui, R.C. Sassonia, K. Dua, I.S. Kikuchi, T. de Jesus Andreoli Pinto, Impact of sterilization methods on electrospun scaffolds for tissue engineering, *Eur. Polym. J.* 82 (2016) 181–195.
- [58] Q. Shi, S.-C. Wong, W. Ye, J. Hou, J. Zhao, J. Yin, Mechanism of adhesion between polymer fibers at nanoscale contacts, *Langmuir* 28 (2012) 4663–4671.
- [59] Q. Shi, Q. Fan, X. Xu, W. Ye, J. Hou, S.-C. Wong, J. Yin, Effect of surface interactions on adhesion of electrospun meshes on substrates, *Langmuir* 30 (2014) 13549–13555.
- [60] C.L. Bowe, L. Mokhtarzadeh, P. Venkatesan, S. Babu, H.R. Axelrod, M.J. Sofia, R. Kakarla, T.Y. Chan, J.S. Kim, H.J. Lee, G.L. Amidon, S.Y. Choe, S. Walker, D. Kahne, Design of compounds that increase the absorption of polar molecules, *Proc. Natl. Acad. Sci.* 94 (1997) 12218–12223.
- [61] M.J. Boeree, N. Heinrich, R. Aarnoutse, A.H. Diacon, R. Dawson, S. Rehal, G.S. Kibiki, G. Churchyard, I. Sanne, N.E. Ntinginya, L.T. Minja, R.D. Hunt, S. Charalambous, M. Hanekom, H.H. Semvua, S.G. Mpagama, C. Manyama, B. Mtshya, K. Reither, R.S. Wallis, A. Venter, K. Narunsky, A. Mekota, S. Henne, A. Colbers, G.P. van Balen, S.H. Gillespie, P.P.J. Phillips, M. Hoelscher, High-dose rifampicin, moxifloxacin, and SQ109 for treating tuberculosis: a multi-arm, multi-stage randomised controlled trial, *Lancet Infect. Dis.* 17 (2017) 39–49.
- [62] K. Fujihara, M. Kotaki, S. Ramakrishna, Guided bone regeneration membrane made of polycaprolactone/calcium carbonate composite nano-fibers, *Biomaterials* 26 (2005) 4139–4147.
- [63] G. Perumal, P.M. Sivakumar, A.M. Nandkumar, M. Doble, Synthesis of magnesium phosphate nanoflakes and its PCL composite electrospun nanofiber scaffolds for bone tissue regeneration, *Mater. Sci. Eng. C* 109 (2020) 110527.
- [64] Z.I. Foraida, T. Kamaldinov, D.A. Nelson, M. Larsen, J. Castracane, Elastin-PLGA hybrid electrospun nanofiber scaffolds for salivary epithelial cell self-organization and polarization, *Acta Biomater.* 62 (2017) 116–127.
- [65] J.I. Kim, T.I. Hwang, L.E. Aguilar, C.H. Park, C.S. Kim, A controlled design of aligned and random nanofibers for 3D bi-functionalized nerve conduits fabricated via a novel electrospinning set-up, *Sci. Rep.* 6 (2016) 1–12.
- [66] G. Onak, M. Şen, N. Horzum, U.K. Ercan, Z.B. Yarah, B. Garipcan, O. Karaman, Aspartic and glutamic acid templated peptides conjugation on plasma modified nanofibers for osteogenic differentiation of human mesenchymal stem cells: a

- comparative study, *Sci. Rep.* 8 (2018) 1–15.
- [67] G. Singh, T. Kaur, R. Kaur, A. Kaur, Recent biomedical applications and patents on biodegradable polymer-PLGA, *Int J Pharm Pharm Sci* 1 (2014) 30–42.
- [68] O. Ivashchenko, T. Tomila, N. Ulyanchich, T. Yarmola, I. Uvarova, Fourier-transform infrared spectroscopy of antibiotic loaded ag-free and ag-doped hydroxyapatites, *advanced science, Eng. Med.* 6 (2014) 193–202.
- [69] Y. Liu, X. Wang, Y. Xu, Z. Xue, Y. Zhang, X. Ning, X. Cheng, Y. Xue, D. Lu, Q. Zhang, F. Zhang, J. Liu, X. Guo, K.-C. Hwang, Y. Huang, J.A. Rogers, Y. Zhang, Harnessing the interface mechanics of hard films and soft substrates for 3D assembly by controlled buckling, *Proc. Natl. Acad. Sci.* 116 (2019) 15368–15377.
- [70] S. Bai, H. Han, X. Huang, W. Xu, D.L. Kaplan, H. Zhu, Q. Lu, Silk scaffolds with tunable mechanical capability for cell differentiation, *Acta Biomater.* 20 (2015) 22–31.
- [71] W.-T. Hsieh, Y.-S. Liu, Y.-h. Lee, M.G. Rimando, K.-h. Lin, O.K. Lee, Matrix dimensionality and stiffness cooperatively regulate osteogenesis of mesenchymal stromal cells, *Acta Biomater.* 32 (2016) 210–222.
- [72] K. Ye, X. Wang, L. Cao, S. Li, Z. Li, L. Yu, J. Ding, Matrix stiffness and nanoscale spatial organization of cell-adhesive ligands direct stem cell fate, *Nano Lett.* 15 (2015) 4720–4729.
- [73] Y. Ding, W. Li, F. Zhang, Z. Liu, N. Zanjanzadeh Ezazi, D. Liu, H.A. Santos, Electrospun fibrous architectures for drug delivery, tissue engineering and cancer therapy, *Adv. Funct. Mater.* 29 (2019) 1802852.
- [74] H. Dickert, K. Machka, I. Braveny, The uses and limitations of disc diffusion in the antibiotic sensitivity testing of bacteria, *Infection* 9 (1981) 18–24.
- [75] W.W. Davis, T.R. Stout, Disc plate method of microbiological antibiotic assay. II. Novel procedure offering improved accuracy, *Appl. Microbiol.* 22 (1971) 666–670.
- [76] Y. Wang, J. Gong, Y. Yao, Extracellular nanofiber-orchestrated cytoskeletal reorganization and mediated directional migration of cancer cells, *Nanoscale* 12 (2020) 3183–3193.
- [77] A. Denchai, D. Tartarini, E. Mele, Cellular response to surface morphology: electrospinning and computational modeling, *Front. Bioeng. Biotechnol.* 6 (2018) 155.
- [78] F. Jahanmard, M.B. Eslaminejad, M. Amani-Tehran, F. Zarei, N. Rezaei, M. Croes, S.A. Yavari, Incorporation of F-MWCNTs into electrospun nanofibers regulates osteogenesis through stiffness and nanotopography, *Mater. Sci. Eng. C* 106 (2020) 110163.
- [79] G.L. Mandell, T.K. Vest, Killing of Intraleukocyte *Staphylococcus aureus* by Rifampin: in-vitro and in-vivo studies, *J. Infect. Dis.* 125 (1972) 486–490.
- [80] D. Baldoni, M. Haschke, Z. Rajacic, W. Zimmerli, A. Trampuz, Linezolid alone or combined with rifampin against methicillin-resistant *Staphylococcus aureus* in experimental foreign-body infection, *Antimicrob. Agents Chemother.* 53 (2009) 1142–1148.
- [81] D.R. Osmon, E.F. Berbari, A.R. Berendt, D. Lew, W. Zimmerli, J.M. Steckelberg, N. Rao, A. Hanssen, W.R. Wilson, Diagnosis and management of prosthetic joint infection: clinical practice guidelines by the Infectious Diseases Society of America, *Clin. Infect. Dis.* 56 (2012) e1–e25.
- [82] F.D. Lowy, D.S. Chang, P.R. Lash, Synergy of combinations of vancomycin, gentamicin, and rifampin against methicillin-resistant, coagulase-negative staphylococci, *Antimicrob. Agents Chemother.* 23 (1983) 932–934.
- [83] C.U. Tuazon, M.Y. Lin, J.N. Sheagren, In vitro activity of rifampin alone and in combination with nafcillin and vancomycin against pathogenic strains of *Staphylococcus aureus*, *Antimicrob. Agents Chemother.* 13 (1978) 759–761.
- [84] P. Vergidis, M.S. Rouse, G. Euba, M.J. Karau, S.M. Schmidt, J.N. Mandrekas, J.M. Steckelberg, R. Patel, Treatment with linezolid or vancomycin in combination with rifampin is effective in an animal model of methicillin-resistant *Staphylococcus aureus* foreign body osteomyelitis, *Antimicrob. Agents Chemother.* 55 (2011) 1182–1186.
- [85] J.A. Niska, J.H. Shahbazian, R.I. Ramos, K.P. Francis, N.M. Bernthal, L.S. Miller, Vancomycin-rifampin combination therapy has enhanced efficacy against an experimental *Staphylococcus aureus* prosthetic joint infection, *Antimicrob. Agents Chemother.* 57 (2013) 5080–5086.
- [86] A. de Breijl, M. Riool, R.A. Cordfunke, N. Malanovic, L. de Boer, R.I. Koning, E. Ravensbergen, M. Franken, T. van der Heijde, B.K. Boekema, The antimicrobial peptide SAAP-148 combats drug-resistant bacteria and biofilms, *Sci. Transl. Med.* 10 (2018) eaan4044.
- [87] R.J. Arts, B. Novakovic, R. Ter Horst, A. Carvalho, S. Bekkering, E. Lachmandas, F. Rodrigues, R. Silvestre, S.C. Cheng, S.Y. Wang, E. Habibi, L.G. Gonçalves, I. Mesquita, C. Cunha, A. van Laarhoven, F.L. van de Veerdonk, D.L. Williams, J.W. van der Meer, C. Logie, L.A. O'Neill, C.A. Dinarello, N.P. Riksen, R. van Crevel, C. Clish, R.A. Notebaart, L.A. Joosten, H.G. Stunnenberg, R.J. Xavier, M.G. Netea, Glutaminolysis and fumarate accumulation integrate immunometabolic and epigenetic programs in trained immunity, *Cell Metab.* 24 (2016) 807–819.
- [88] M. Croes, M.C. Kruij, W. Boot, B. Pouran, M. Braham, S. Pakpahan, H. Weinans, H. Vogely, A.C. Fluit, W. Dhert, The role of bacterial stimuli in inflammation-driven bone formation, *Eur. Cells Mater.* 37 (2019) 402–419.
- [89] K. Malizos, M. Blauth, A. Danita, N. Capuano, R. Mezzoprete, N. Logoluso, L. Drago, C.L. Romano, Fast-resorbable antibiotic-loaded hydrogel coating to reduce post-surgical infection after internal osteosynthesis: a multicenter randomized controlled trial, *J. Orthop. Traumatol.* 18 (2017) 159.
- [90] S. Bakhshandeh, S. Amin Yavari, Electrophoretic deposition: a versatile tool against biomaterial associated infections, *J. Mater. Chem. B* 6 (2018) 1128–1148.
- [91] J.-A. Park, K.Y. Cho, C.H. Han, A. Nam, J.-H. Kim, S.-H. Lee, J.-W. Choi, Quaternized amphiphilic block copolymers/graphene oxide and a poly (vinyl alcohol) coating layer on graphene oxide/poly (vinylidene fluoride) electrospun nanofibers for superhydrophilic and antibacterial properties, *Sci. Rep.* 9 (2019) 383.
- [92] A.G. Gristina, Biomaterial-centered infection: microbial adhesion versus tissue integration, *Science* 237 (1987) 1588–1595.
- [93] A. Sheikhi, J. Hayashi, J. Eichenbaum, M. Gutin, N. Kuntjoro, D. Khorsandi, A. Khademhosseini, Recent advances in nanoengineering cellulose for cargo delivery, *J. Control. Release* 294 (2019) 53–76.
- [94] M. Bartnikowski, T.R. Dargaville, S. Ivanovski, D.W. Hutmacher, Degradation mechanisms of polycaprolactone in the context of chemistry, geometry and environment, *Prog. Polym. Sci.* 96 (2019) 1–20.
- [95] A. Sohrabi, P.M. Shaibani, H. Etayash, K. Kaur, T. Thundat, Sustained drug release and antibacterial activity of ampicillin incorporated poly(methyl methacrylate)-nylon6 core/shell nanofibers, *Polymer* 54 (2013) 2699–2705.
- [96] N.B. Damm, M.M. Morlock, N.E. Bishop, Friction coefficient and effective interference at the implant-bone interface, *J. Biomech.* 48 (2015) 3517–3521.
- [97] A.V. Carli, A.S. Sethuraman, S.J. Bhimani, F.P. Ross, M.P. Bostrom, Selected heat-sensitive antibiotics are not inactivated during polymethylmethacrylate curing and can be used in cement spacers for periprosthetic joint infection, *J. Arthroplast.* 33 (2018) 1930–1935.
- [98] W.-S. Kim, I.-H. Yun, J.-J. Lee, H.-T. Jung, Evaluation of mechanical interlock effect on adhesion strength of polymer-metal interfaces using micro-patterned surface topography, *Int. J. Adhes. Adhes.* 30 (2010) 408–417.
- [99] J. Bobyn, G. Stackpool, S. Hacking, M. Tanzer, J. Krygier, Characteristics of bone ingrowth and interface mechanics of a new porous tantalum biomaterial, *J. Bone Joint Surg.* 81 (1999) 907–914 British volume.
- [100] S. Amin Yavari, J. van der Stok, S.M. Ahmadi, R. Wauthle, J. Schrooten, H. Weinans, A.A. Zadpoor, Mechanical analysis of a rodent segmental bone defect model: the effects of internal fixation and implant stiffness on load transfer, *J. Biomech.* 47 (2014) 2700–2708.
- [101] S.A. Yavari, J. van der Stok, Y.C. Chai, R. Wauthle, Z.T. Birgani, P. Habibovic, M. Mulier, J. Schrooten, H. Weinans, A.A. Zadpoor, Bone regeneration performance of surface-treated porous titanium, *Biomaterials* 35 (2014) 6172–6181.
- [102] M. Croes, B. Akhavan, O. Sharifmadian, H. Fan, R. Mertens, R.P. Tan, A. Chunara, A.A. Fadzil, S.G. Wise, M.C. Kruij, S. Wijdicks, W.E. Hennink, M.M.M. Bilek, S. Amin Yavari, A multifaceted biomimetic interface to improve the longevity of orthopedic implants, *Acta Biomater.* 110 (2020) 266–279.
- [103] Y. Dong, T. Yong, S. Liao, C.K. Chan, M.M. Stevens, S. Ramakrishna, Distinctive degradation behaviors of electrospun polyglycolide, poly(DL-lactide-co-glycolide), and poly(L-lactide-co-epsilon-caprolactone) nanofibers cultured with/without porcine smooth muscle cells, *Tissue Eng. A* 16 (2010) 283–298.
- [104] J. Dulnik, Biodegradation of bicomponent PCL/gelatin and PCL/collagen nanofibers electrospun from alternative solvent system, *Polym. Degrad. Stab.* 130 (2016) 10-21-2016 v.2130.